Pseudophosphatase STYX modulates cell fate decisions and cell migration by spatiotemporal regulation of ERK1/2

Veronika Reiterer[1*], Dirk Fey[2*], Walter Kolch[2], Boris N. Kholodenko[2#], Hesso Farhan[1, 3, #]

1 Biotechnology Institute Thurgau at the University of Konstanz, Kreuzlingen, Switzerland

2 Systems Biology Ireland and School of Medicine and Medical Science, University College Dublin, Belfield, Dublin 4, Ireland

3 Department of Biology, University of Konstanz, Universitätsstrasse 10, D-78547 Konstanz, Germany

* These authors contributed equally to this work.

#Corresponding author: hesso.farhan@uni-konstanz.de

Corresponding author: boris.kholodenko@ucd.ie

Abstract

Serine/threonine/tyrosine-interacting protein (STYX) is a catalytically inactive member of the dual-specificity phosphatases (DUSPs) family. Whereas the role of DUSPs in cellular signaling is well explored, the function of STYX is still unknown. Here, we identify STYX as a spatial regulator of ERK signaling. We used predictive model simulation to test several hypotheses for possible modes of STYX action. We show that STYX localizes to the nucleus, competes with nuclear DUSP4 for binding to ERK and acts as a nuclear anchor that regulates ERK nuclear export. Depletion of STYX increases ERK activity in both cytosol and nucleus. Importantly, depletion of STYX causes an ERK-dependent fragmentation of the Golgi apparatus and inhibits Golgi polarization and directional cell migration. Finally, we show that overexpression of STYX reduces ERK1/2 activation, thereby blocking PC12 cell differentiation. Overall, our results identify STYX as an important regulator of ERK1/2 signaling critical for cell migration and PC12 cell differentiation.

\body

Introduction

Extracellular regulated kinases (ERK1 and -2, referred to as ERK from here on) phosphorylate more than 200 known substrates (1, 2), and therefore play a central role in numerous cellular processes such as proliferation, differentiation, or motility. The upstream kinases MEK1/2 not only activate ERK, but also are involved in spatial regulation by acting as cytosolic anchors for ERK. Interestingly, substrate binding in the nucleus has a similar anchoring role delaying ERK nuclear exit and protecting against inactivation by phosphatases (3). In addition, scaffold proteins were shown to regulate spatiotemporal ERK signaling by bringing kinases to certain subcellular locations, such as endosomes (by p14;(4)) or to the Golgi apparatus (by Sef1; (5)). Finally, dephosphorylation of active ERK by (DUSPs) plays and important role in the regulation of ERK signaling in both time and space(6). The human genome encodes at least 25 constitutively expressed or inducible DUSPs, which can be subdivided based on their subcellular location (mainly cytosolic, mainly nuclear, or both) and specificity toward the various MAPK members. Catalytic activity is conferred by a cysteine residue that is part of a conserved motif (I/VH***C***XAGXXR). Despite considerable progress made by exploring in vitro substrate specificity and expression profile of DUSPs, we still do not fully understand many of their functions at the level of cell biology. Even more enigmatic are the catalytically inactive DUSP family members (pseudophosphatases), which share the conserved catalytic domain but lack the critical cysteine residue.

In the current work we focus on the pseudophosphatase STYX the role of which in the regulation of ERK has been unexplored. STYX was first described as an inactive DUSP, in which the catalytic cysteine at position 120 is replaced by glycine (7). Mutation of G120 back to cysteine restored catalytic activity. Male mice knocked-out for STYX display a defect in spermatogenesis (8), and, to date, the only protein shown to interact with STYX is Carhsp24, a phosphoprotein involved in the translational repression of histone mRNAs. Thus, STYX

remains an enigmatic protein and none of the previous work could establish a link to MAPK signaling in general or ERK signaling in particular. The goal of this work was to identify and characterize a potential role of STYX in ERK signaling. Although computational modeling is often used to confirm experimental findings, we used modeling as a discovery tool. Embracing the principle ways of how STYX might interact with ERK, our models generated salient predictions that we next tested experimentally. We find that STYX directly binds ERK in the nucleus, thereby acting as an anchor that modulates the nucleocytoplasmic shuttling of this MAPK. Moreover, STYX competes with nuclear DUSPs for binding to ERK, thus modulating the ability of catalytically active DUSPs to access ERK. We demonstrate that the STYX-ERK interaction modulates the biologic outcome of ERK activation by regulating both directional cell migration and cell fate decisions.

Results

Building core models for testing the mode of action of STYX

We use biochemical experiments and computational modeling to delineate the role of STYX in the control of spatiotemporal ERK dynamics. The complexity of the regulation of cell signaling is often difficult to grasp intuitively, especially when trying to integrate the spatial and dynamic aspects. Based on alternative feasible hypotheses about STYX action, we build several computational models to, first, explore the emerging network properties on a systems level and, second, test these predictions against experimental data. The common core of our models (Fig. 1A) is based on established, well calibrated models of (i) ERK activation by MEK in the cytoplasm (where ERK is phosphorylated at two distinct phosphorylation sites in its kinase domain), (ii) shuttling of differentially phosphorylated ERK forms in and out of the nucleus and (iii) dephosphorylation of phospho-ERK by DUSPs in the cytoplasm and the nucleus, where the nuclear DUSP induction by active ERK is incorporated in our models (*see Material and Methods and the Supplement for more details*).

Further integrating STYX into a computational model of ERK signaling requires information on the spatial localization of STYX. Therefore, we determined the subcellular localization of STYX. Both overexpressed and endogenous STYX localized mainly to the cell nucleus, with little staining also visible in the cytosol (Fig. 1 B and C). The localization pattern did not differ between nonstimulated and stimulated cells (Fig. 1B&C). Because the expression of some nuclear DUSPs is induced by ERK signaling, we also tested the expression of STYX in cells that were serum-starved and compared it to stimulated cells. STYX levels did not change for up to 60 min upon serum stimulation, whereas the expression of DUSP4 (a nuclear inducible DUSP) was markedly induced (Fig. S1). Finally, we tested whether STYX is actually a pseudophosphatase. The validation of this assumption is important because the lack of catalytic activity of STYX was only demonstrated with the purified STYX protein and artificial substrates (p-nitrophenolphosphate and phosphorylated small peptides) (7). Moreover, STYX may have an unknown interaction partner that could mediate catalytic activity, which cannot be observed when using the purified STYX protein. However, using an immunoprecipitate of STYX from cells is supposed to include all hypothetical cofactors. Therefore, we immunoprecipitated STYX from cells and tested its ability to dephosphorylate purified double-phosphorylated (pp)ERK2. In contrast to immunoprecipitated DUSP4 which strongly dephosphorylated ppERK2, STYX was devoid of such an activity (Fig. S2). STYX is inactive because of the absence of a critical cysteine residue at position 120 which is replaced by a glycine residue. It was previously shown that mutation of the Gly^{120} back to cysteine resulted in a protein that is capable of dephosphorylating the artificial substrate p-nitrophenolphosphate (7), but it was never tested whether STYX-G120C is capable of dephosphorylating ppERK. We generated the same mutant (STYX-G120C) and compared the activity of this mutant with wild type STYX toward ppERK2. While the wild type protein did not dephosphorylate ERK2 to any appreciable extent, STYX-G120C readily dephosphorylated ppERK2 (Fig. 1D). This result is

in line with the notion that STYX is catalytically inactive due to the absence of a cysteine residue at position 120. Therefore, we conclude that STYX is a noninducible pseudophosphatase that localizes predominantly to the nucleus.

Based on this information and our core model, we build five different hypothetical models of how STYX might act. These models are schematically depicted in Fig. 1A (for simplicity only unphosphorylated and double-phosphorylated ERK forms are shown). A detailed description of these models, as well as parameter refinement procedures are provided in the *Supplementary Material* (see Fig. S3, the Supplementary text and Tables S1 and S2). In model 1, STYX binds both phosphorylated and unphosphorylated forms of ERK in the nucleus, whereas models 2 and 3 assume that STYX binds only unphosphorylated ERK or only ppERK, respectively. Model 4 assumes that STYX imports ppERK from the cytosol to the nucleus. Model 5 assumes that STYX exports unphosphorylated ERK. Using these models we next tested the behavior of the system under control and STYX-depleted conditions (Fig. 1A).

Experimental testing of the predictions rules out some models

In the different models, depletion of STYX affected the ERK activation dynamics differently (Fig. 1A). When we knocked down STYX expression in HeLa cells, we observed a marked increase of ppERK in response to serum treatment as measured in total cell lysates (Fig. 2A). The same was true when we stimulated HeLa cells with EGF or with phorbolester (Fig. S4A&B), indicating that the effect is not stimulus-specific. Moreover, we obtained similar results when we performed the STYX knockdown in HEK293 cells or HepG2 cells (Fig. S4C&D), indicating that the effect of STYX on ERK signaling is not confined to a certain cell line. Furthermore, this effect was not confined to a single ERK isoform (Fig. S5). The observed increase of ppERK allows us to reject models 3 & 5. In model 3, where STYX binds exclusively ppERK, the STYX knockdown prevents the accumulation of STYX-ppERK

complexes, thus predicting a decrease of overall ppERK levels. In model 5 the knockdown of STYX slows down the export of unphosphorylated ERK, de-facto delaying ERK re-phosphorylation and thus decreasing ppERK levels in both, the cytosol and the nucleus. The predicted trajectories of model 1 best simulated the time-course data following the STYX knockdown, but models 2 and 4 also predicted a significant increase of the ERK activation dynamics. Consequently, from this point on we consider only models 1, 2 and 4.

STYX depletion increases both cytosolic and nuclear ERK activities

In contrast to models 1 and 2, model 4 predicted a decreased nuclear ERK activity in response to STYX depletion (Fig. 2B). To test these predictions, we measured the phosphorylation status of two well established ERK substrates in the cytosol and nucleus. In STYX knockdown cells serum treatment resulted in an increased phosphorylation of cytosolic (p-RSK; Fig. 2C) as well as nuclear (p-Elk1; Fig. 2D) substrates. Thus, STYX depletion increases ERK activity in both the cytosol and nucleus and based on this we reject model 4.

STYX binds both unphosphorylated and phosphorylated forms of ERK

The key difference between the remaining models 1&2 is the differential STYX binding to the various phosphorylation forms of ERK. In order to further analyze these models, we first need to demonstrate that STYX binds ERK and that this interaction is direct. To visualize the interaction, we used a YFP-complementation assay (YPCA), where the two severed halves of YFP were fused to STYX and ERK2. In case of interaction, the two YFP fragments are brought into close proximity, leading to complementation of the intact YFP molecule and emission of a fluorescent signal. HeLa cells expressing YFP2-STYX and YFP1-ERK2 were fixed and the complex formation was analyzed by fluorescence microscopy. The complex formed by YFP2-STYX and YFP1-ERK2 localized to the nucleus and only partly to the cytosol (Fig. 2E), indicating that the nucleus is the main site of interaction of STYX and

ERK2. To provide evidence for a direct interaction, we tested the interaction of STYX and ERK2 using pure components. In vitro translated YFP2-STYX interacted with recombinant and purified GST-ERK2 (Fig. 2F). Finally, we also tested the interaction of purified His-tagged STYX with purified GST-tagged ERK2 and further confirmed that the interaction of the two proteins is direct (Fig. S6).

We next wanted to distinguish model 1 (STYX binds both phosphorylated and unphosphorylated ERK) from model 2 (STYX binds only the unphosphorylated ERK). If STYX exhibits differential binding, then the coimmunoprecipitation between STYX and ERK ought to change in response to stimulation. Therefore, we performed coimmunoprecipitation experiments of YFP-tagged STYX with flag-tagged ERK2. We compared cells that were serum-starved for 2-3 hours (very low level of ppERK) with cells that were stimulated with serum for 15 min (high levels of ppERK). In addition, we also included cells from steady-state conditions (moderate levels of ppERK). Regardless of the condition used, the same levels of ERK2 co-immunoprecipitated with STYX (Fig. 2G), which indicates that the interaction is insensitive to the levels of ppERK2 and thus supports the conclusion that STYX binds to ERK regardless of its phosphorylation status. This finding is not only inconsistent with model 2, but also provides further grounds to reject model 4 in which STYX would preferentially bind to ppERK in the cytoplasm and import ppERK into the nucleus, as well as model 5 in which STYX would preferentially bind to the nuclear ERK and export it from the nucleus. Taken together, the only model consistent with all our experimental observations is model 1.

Calibration of model 1 validates its accuracy

Model 1 is the only model qualitatively consistent with all of our observations. Next, we asked how well it can explain the ppERK time-course data quantitatively. Therefore, we trained the model to fit the data using a global parameter estimation method called adaptive

simulated annealing (see *Material and Methods* & Supplement for details). For fitting we used a training data set containing the ppERK time-courses in control and STYX knockdown conditions, but not the STYX overexpression data which were used later for model validation. We found that model 1 can indeed explain these data [Fig. 3A, based on our estimation results and a Pearsons's X^2 test (9), the probability that the model conforms with the data is P = 0.88]. Furthermore, despite the fact that some parameter values were not uniquely identifiable, their correlations could be estimated accurately (Fig. 3B), which in turn resulted in accurate predictions of the ppERK time-course in STYX overexpressing cells (Fig. 3C&D). The fact that model 1 was capable of quantitatively explaining the STYX knockdown data and, in addition, accurately predicted the STYX overexpression time-course further strengthened our confidence in this model.

Testing predictions of the validated model shows that STYX acts as a nuclear anchor for ERK

Both, modeling and the experimental data support a role of STYX as a nuclear anchor for ERK. To experimentally test whether STYX is a nuclear anchor for ERK1/2, we first performed biochemical fractionation experiments to test for the distribution of endogenous ERK in control and STYX knockdown cells. Consistent with the notion that STYX is a nuclear anchor, ERK was found to be more abundant in the cytosol of STYX depleted cells (Fig. 4A). Our model (model 1) predicted that STYX depletion would increase the rate of ERK efflux from the nucleus to the cytosol (Fig. 4B). Therefore, we next used fluorescence recovery after photobleaching (FRAP) microscopy to evaluate the effect of STYX depletion and overexpression on the rate of ERK1/2 shuttling out of the nucleus. The cytosol of cells expressing GFP-ERK2 was bleached and recovery of fluorescence was monitored. This fluorescence recovery can only occur through GFP-ERK transport from the nonbleached nucleus and therefore reflects the rate of GFP-ERK2 export from the nucleus to the cytosol. In

concordance with the model prediction, the extent of ERK2 export from the nucleus was significantly higher in STYX knockdown cells when compared to control (Fig. 4C). Although these FRAP experiments revealed the subcellular dynamics of ERK, the use of GFP-ERK2 did not allow us to distinguish between free and STYX-bound ERK. To that end we performed a combined FRAP-YPCA experiment in cells expressing YFP2-STYX and YFP1-ERK2. Because the complementation of YFP1&2 is kinetically irreversible, this setup permanently links the STYX-ERK complexes. Consequently the recovery of fluorescence after bleaching the cytosol can only arise from nonbleached STYX-ERK complexes leaving the nucleus. The recovery of the cytosol in these cells was very weak, indicating that the transport of STYX-ERK complexes from the nucleus to the cytosol is negligible (Fig. S7). Taken together these data support the conclusion that STYX acts as a nuclear anchor for ERK.

STYX competes with DUSP4 for binding to ERK2

Our results are consistent with a model where STYX binds all ERK forms and sequesters them in the nucleus. A consequence of this is that STYX competes with nuclear DUSPs for binding to ERK. Therefore, we tested whether STYX competes with DUSP4, a nuclear inducible DUSP, for binding to ERK using coimmunoprecipitation experiments. As shown in Fig. 5A, overexpression of DUSP4 reduces the amount of STYX in the ERK2 IP, suggesting that DUSP4 replaces STYX in the complex with ERK2. We also used the YPCA as an independent method to test for competition between STYX and DUSP4. STYX and ERK2 formed a complex that mainly localized to the nucleus. Titrating increasing amounts of DUSP4 into these cells reduced the fluorescence signal (Fig. 5B), indicating that less ERK2-STYX complexes are formed in the presence of increasing DUSP4 levels. Competition between STYX and DUSP4 was also observed when the experiment was performed in cells stimulated with serum (Fig. S8A). STYX and DUSP4 also exhibited competition toward a catalytically inactive mutant of ERK2 (ERK2-K52R) (Fig. S8B). We also tested whether

STYX and DUSP4 compete for binding to a nonphosphorylatable ERK2 mutant and therefore mutated the dual-phosphorylation site (threonine to alanine and tyrosine to phenylalanine) on ERK2 (ERK2-TYAF) and tested whether STYX and DUSP4 compete for binding to this mutant, which was not phosphorylated upon serum stimulation (Fig. S9) but is still capable of binding to ERK2 in a manner comparable to that observed with wild type ERK2 and ERK2-K52R, although the latter tended to exhibit more binding of DUSP4 (Fig. S10). STYX also competed with DUSP4 for binding to ERK2-TYAF (Fig. S8C). These results further support that STYX binds to ERK in a manner independent of phosphorylation. The seven-maker mutant of ERK2 (ERK2-D319N) does not bind DUSPs (10-14). If STYX and DUSP4 compete for binding to ERK, then their binding modes are likely to be analogous and sensitive to mutation of D319 in ERK. As shown in Fig. 5C, ERK2-D319N is unable to coimmunoprecipitate with STYX, thus indicating that STYX and DUSP4 share the same binding site on ERK. Taken together we conclude that DUSP4 and STYX compete for binding to ERK in the nucleus thus, substantiating the conclusion that STYX is a nuclear anchor for ERK.

Effect of STYX depletion on Golgi structure and cell migration

ERK signaling plays a key role in the regulation of many cellular processes, including directional cell migration. Upon initiation of directional motility, the cell polarizes the Golgi apparatus toward the leading edge in a manner dependent on ERK-induced phosphorylation of Golgi matrix proteins (15). Disruption of the structural integrity of the Golgi, results in an inhibition of cell migration (15, 16). In our previous work we identified STYX as a potential regulator of the Golgi structure (17). Depletion of STYX was shown to result in fragmentation of the Golgi apparatus, but this effect was not assessed quantitatively and the underlying mechanism was not explored. In light of the observation that ERK directly signals to the Golgi (15), we asked whether the effect of STYX on ERK signaling is causally linked to

alteration of Golgi morphology. As shown in Fig. 6A, the Golgi represents a single copy organelle in control cells, with only a minor fraction of cells exhibiting a fragmented Golgi apparatus. In STYX knockdown cells, the number of cells exhibiting a fragmented Golgi increased by two-fold. This effect could be blocked by pretreatment with PD98059 an inhibitor of MEK-mediated ERK activation (Fig. 6A), demonstrating that ERK signaling is required for the STYX effect.

Next, we asked whether STYX depletion and its disruption of the Golgi structure would also affect directional cell migration. We addressed this question using a wound healing assay, where cells (on glass coverslips) are plated into two chambers separated by a bridge of 600 µm width. After removal of the bridge, cells on both sides start migrating to close the gap. Wound closure was slower in STYX knockdown cells, which migrated on average 100 µm less over a time scale of 18 h (Fig. 6B). We determined the orientation of the Golgi apparatus towards the leading edge and found that depletion of STYX strongly inhibited directional polarity of the Golgi (Fig. 6C). Our results demonstrate that STYX disrupts the Golgi structure in an ERK dependent manner and thereby affects directional cell migration.

STYX modulates cell fate decisions

ERK controls a plethora of cell responses to external and internal cues, including cell fate decisions. For instance, the duration of ERK signaling in PC12 cells, determines whether these cells will proliferate or differentiate (18, 19). Treatment of PC12 cells with EGF results in a transient ERK activation that returns to basal levels at 60 min after stimulation leading to cell proliferation. A prolonged ERK response observed after treatment with nerve growth factor (NGF) stops proliferation and initiates differentiation, manifested by the formation of neurite-like extensions. We asked whether overexpression of STYX in PC12 cells, would lower the levels of ppERK. We focused on the late phase (60 min) after NGF treatment,

because, at this is a time point, there is a marked difference in ppERK between NGF and EGF treated cells. Similarly as in HeLa cells, overexpression of STYX also reduced the levels of ppERK in PC12 cells at 60 min after NGF treatment (Fig. 7A). Next, we asked whether the decreased level of ppERK in the late phase would affect differentiation of PC12 cells in response to NGF. First, we assessed the effect of STYX on GATA transcriptional activity, because earlier findings showed that the effect of ERK on PC12 cell differentiation is also dependent on restoring GATA transcriptional activity (20). Overexpression of STYX resulted in a lower activity of a GATA luciferase reporter (Fig. S11). Next we assessed the effect of STYX overexpression on the ability of PC12 cell to form neurite-like extensions. Overexpression of STYX strongly reduced the amount of differentiated PC12 cells (Fig. 7B), indicating that STYX is able to modify cell-fate decisions through the control of ERK signaling.

Discussion

In the current work we identify the pseudophosphatase STYX as a regulator of ERK signaling. Owing to its importance in regulating cell proliferation, cell migration and cell fate decisions, understanding the regulation of ERK signaling in time and space is central for the design of novel therapeutic strategies against human pathologies. For instance, directional cell migration is thought to constitute the cellular basis for invasion and metastatic dissemination of cancer cells, which accounts for 90% of cancer-associated mortality (21). Our work shows that STYX regulates ERK signaling, which translates into the modulation of cell migration and fate decisions.

It has long been unclear whether and how pseudophosphatase members of the DUSP family are linked to MAPK signaling. For instance DUSP24 (also known as MK-STYX) has been shown to regulate apoptosis and to inhibit stress granule formation, but no role in the regulation of MAPK signaling has been described. Here we show that STYX acts as a nuclear

anchor for ERK, effectively slowing its nuclear export. In the absence of STYX, ERK leaves the nucleus with faster dynamics, which permits reactivation of ERK in the cytosol, thus causing increased cytoplasmic and nuclear ERK activities. This interpretation is supported by our computational modeling. In contrast to other feasible models of STYX actions, a model in which STYX acts as a nuclear anchor faithfully predicted all our experimental findings. The concept that an inactive phosphatase might act as an anchor for ERK has been proposed when it was shown that an artificially inactivated version of the nuclear DUSP5 may function as a nuclear anchor for ERK (22). Here, we here identify STYX as a naturally occurring dead phosphatase that acts as a nuclear anchor.

Both, our computational modeling and our experimental results indicate that STYX competes with nuclear DUSP4 for binding to ERK and that this competition is part of the mode of action of STYX. It was recently shown that Mxi2 also acts as a competitor of nuclear DUSPs, thereby preventing ERK dephosphorylation (23). The effects of STYX and Mxi2 on ERK signaling are totally different, despite that they both compete with nuclear DUSPs for binding to ERK. Overexpression of Mxi2 increases ERK signaling and the depletion of Mxi2 seems to decrease ERK signaling. Exactly the opposite is observed for STYX (its overexpression inhibits and its depletion increases ERK signaling). Another difference is that Mxi2 seems to specifically regulate nuclear ERK activity whereas STYX affects both, cytosolic and nuclear ERK activities. Possible reasons for the difference between Mxi2 and STYX are the fact that Mxi2 promotes entry of active ERK to the nucleus (23, 24), whereas we have no evidence that STYX exerts direct effects on the ERK transport. Depletion of a nuclear importer of active ERK is predicted to decrease the amount of nuclear ppERK (model 4). Thus, it is likely that the difference between STYX and Mix2 is that the latter promotes the nuclear entry of ERK. Moreover, STYX binds both to nonphosphorylated ERK and ppERK and our modeling indicates that this fact is important to explain the experimental findings. It is unclear whether Mxi2 exhibits any preference toward different phosphorylation forms of

ERK. However, a strong difference in the binding to phosphorylated *vs.* non-phosphorylated ERK could potentially also account for the difference between STYX and Mxi2.

Our data strongly suggest that STYX depletion affects Golgi structure via increased ERK signaling. It has been previously shown that ERK phosphorylated the Golgi matrix protein GRASP65, thereby allowing the Golgi to reorient towards the leading edge in migrating cells. Phosphorylation of GRASP65 was shown to result in unlinking from other Golgi matrix proteins, which results in structural rearrangements of the Golgi (25). Therefore interphase ERK signaling is capable of phosphorylating the Golgi in addition to the ERK1c form that was shown to phosphorylate the Golgi as part of mitotic disassembly of the Golgi (26). Further evidence that hyperactive ERK in interphase cells favors fragmentation of the Golgi was provided recently by showing that DUSP6 knockdown, which hyperactivates ERK (27), results in Golgi fragmentation, which could be rescued by pharmacologically inhibiting ERK (28).

Typically, an increase of ERK activity is considered to support tumorigenesis. Yet, our finding place STYX as a potential therapeutic target, because the fragmentation of the Golgi would inhibit directional cell migration and invasion and thereby render cancer cells less capable of invasion and metastatic spreading. A further link between STYX and cancer may also be inferred from its crosstalk with DUSP4. Recent studies showed that DUSP4 can have both detrimental and beneficial effects. On one hand, increased DUSP4 expression was found to be increased in colorectal cancer specimens with high frequency of microsatellite instability indicating poor survival rates (29). On the other hand, DUSP4 deficiency in breast cancer patients attenuated their response to chemotherapy (30). Taking the crosstalk with STYX into account might help to explain these apparently opposing DUSP4 effects. In any case, we propose that understanding the STYX-ERK-DUSP4 crosstalk is critical for fully understanding the impact of dysregulated ERK signaling on human pathologies.

Materials and Methods

Antibodies and reagents. The following rabbit polyclonal antibodies were purchased from Cell Signaling: ERK1/2, phosphorylated ERK1/2, phosphorylated Elk1, phosphorylated RSK1. Anti-GM130 antibody (mouse monoclonal) was from BD Biosciences. Antibodies against STYX (rabbit polyclonal), against DUSP4 (rabbit polyclonal) and against GFP (rabbit polyclonal) were obtained from Abcam. Anti-flag epitope antibody was from Sigma-Aldrich. Mouse monoclonal anti-GFP antibody was from Roche. Anti-Giantin antibody (rabbit polyclonal) was from Covance Purified STYX was obtained from Abcam. Purified GST-ERK2 was purchased from Cell Signaling. All chemical (unless indicated otherwise) were from Sigma-Aldrich. Collagen-IV was obtained from BD Biosciences.

Plasmids. STYX cDNA was amplified from a human brain library (Invitrogen) using the following primer pairs hSTYX_fw ATGGAGGACGTGAAGCTGGAGTTC and hSTYX _rev: TCAGCCATTCTGTGCAGTCGCC. The PCR product was cloned into a pcDNA3.1 vector. The construct was verified by sequencing. STYX was subloned into pCMV-HA to yield HA-STYX, into YFP2-pcDNA3 to yield YFP2-STYX, into YFP1-pcDNA3 to yield YFP1-STYX, and into pEYFP-C1 vector to yield YFP-STYX. The expression vector for GFP-ERK2 was a kind gift from Dr. Rony Seger (Weizman Institute, Israel). Expression vector for flag-ERK2 and flag-ERK2-D319N were kind gifts from Dr. Melanie Cobb (UT Southwestern Medical Center, Dallas, USA). Expression vector for DUSP4 was a kind gift from Stephen Keyse (Univ. Dundee, UK).

Transfections and MAPK activation assays. In case of siRNA transfection, cells were plated at a density of 2.10^5 in 6-well plates. Cells were transfected with siRNA (10 nM final concentration) using HiPerFect (Qiagen) according to manufacturer's instructions. siRNAs were purchased either from Thermo Fischer (ONTarget SMART pool) or from Qiagen (non pooled siRNAs. After 72 h, cells were serum-starved for 2 h followed by stimulation as

indicated. At defined time points cells were lysed in MAPK buffer (50mM Tris-HCl pH7.4, 10nM EDTA, 100mM NaCl, 0.1% SDS and 1% NP40) supplemented with proteinase inhibitor (cOmplete Mini, Roche) and phosphatase inhibitor (PhosSTOP, Roche). Samples were loaded on polyacrylamide gels followed by immunoblotting. In case of overexpression, cells were plated at a density of 3.10^5 in 6-well plates. On the next day, cells were transfected using Fugene 6 (Promega) according to the manufacturer's instructions.

Co-immunoprecipitation assay. HeLa cells ($3.5x10^6$) were seeded in a 10cm plate and the next day transfected with the indicated plasmids. 24h after transfection cells were harvested and lysed in MAPK-IP buffer (50mM Tris-HCl pH 7.4, 10% glycerol, 150mM NaCl, 2mM EDTA and 0.5% Tx-100) supplemented with proteinase inhibitor (cOmplete Mini, Roche) and phosphatase inhibitor (PhosSTOP, Roche). Lysates were centrifuged for 12 min at 18000xg at 4°C and 3% of the supernatant was removed as an input control. The remaining lysate was incubated with the appropriate resin (for IP against flag tagged proteins: lysate was incubated EZview™ Red ANTI-FLAG M2 affinity gel (Sigma-Aldrich); for IP against HA-tagged proteins, the lysate was incubated with monoclonal anti-HA agarose) overnight. Agarose beads were washed three times and proteins were eluted in 2x reducing loading buffer.

In vitro translation of STYX and binding to GST-ERK2. YFP2 tagged STYX or an YFP2 only containing vector were in vitro translated using the TNT® Quick coupled Transcription/Translation Systems (Promega) according to the manufacturer's instruction. In vitro translated proteins were incubated with protein G sephaose precoupled with anti-GFP antibody overnight at 4°C in MAPK-IP buffer. On the next day, samples were washed and incubated with 0.8ug GST-ERK2 (Sigma-Aldrich) for 2 h in GST buffer (20mM Tris-HCl pH 7.5, 0.2mM EDTA, 0.1M NaCl, 1mM DTT) supplemented with proteinase inhibitors at 4°C. Samples were washed with GST-buffer supplemented with 0.1% NP-40 and eluted in 2x reducing loading buffer.

Subcellular fractionation. $2x10^6$ HeLa cells were seeded in 10cm plate and reverse transfected

with siRNA. 72 h after seeding cells were serum-starved for 2h and subsequently stimulated with 10% FCS for the indicated time. Cells were harvested and the nuclear and cytsolic fractions were prepared using the nuclear extract kit from Active Motif® according to the manufacturer's instructions.

PC12 differentiation and ppERK staining. Cells were plated at a density of 50000 cells on collagen coated glass slides in 12-well plates. PC12 cells were transfected using FugeneHD (Roche) according to manufacturer's instructions. Differentiation was initiated by cultivating the cells in RPMI medium supplemented with 1% horse serum and 50ng/ml NGF (Sigma Aldrich). Cells were scored as differentiated if they exhibited at least one neurite that was longer than one cell diameter. Staining of ppERK in PC12 cells was based on a protocol described by others (31). Briefly, cells were washed with PBSD followed by fixation in 4% paraformaldehyde and 4% sucrose for 20 min at RT. After washing with PBSG (PBS, pH 7.4 with 20mM glycine) cells were permeabilized with PBS containing 0.2% tritonX100 for 15 min at RT . Cells were washed and non specific binding was blocked using 3% goat serum and 0.5% BSA in PBS for 1 h at RT. Anti ppERK antibody (diluted 1:250 in 2.5% goat serum) was incubated over night at 4°C. After washing cells were incubated with secondary antibody (in 2.5% goat serum), followed by washing and embedding.

Microscopy. All microscopy experiments were performed on a Leica-SP5 confocal laser scanning microscope. For FRAP experiments cells on 18 mm glass coverslips were placed into a Ludin chamber type-1 (Life Imaging Services, Switzerland) and the FRAP experiment was performed at 37°C using a 63x immersion oil objective. For bleaching of cytosol, a cell was chosen, the image digitally magnified by 2 fold. The cytosolic area was bleached for 20 sec and fluorescence recovery was acquired at a speed of 1 frame per second for 1 min. Images were analyzed using the ImageJ software.

Immunofluorescence. Cells were fixed using 4% paraformaldehyde (pH 7.4) for 20 min at room temperature. Cells were washed in PBSG (PBS, pH 7.4 with 20mM glycine) and

permeabilized (PBSG with 0.2% triton X100) for 4 min at room temperature followed by washing with PBSG. The primary antibody was diluted in PBSG with 3% BSA (bovine serum albumin) and incubated for 30 min at room temperature followed by washes in PBS. The secondary antibody was diluted in PBS with 3% BSA and incubated for 30 min at room temperature. Slides were washed PBS and mounted using polyvinylalcohol (Sigma).

Core model of ERK signaling. The common core of our models (Fig. S3) is based on the established, well calibrated models of ERK signaling. First, active MEK binds ERK in the cytosol and phosphorylates ERK at two distinct phosphorylation sites in the kinase domain of ERK following a distributive two-collision mechanism (32-34) Second, all differentially phosphorylated forms of ERK can shuttle into and out of the nucleus with the rates given in Table S1 (35). Third, cytosolic and nuclear DUSPs bind and dephosphorylate ERK in their respective compartments, whereas the expression of nuclear DUSP is induced by the nuclear ERK activity (36-38). A detailed account of all reactions in the model is given in Table S1. A successful modeling strategy keeps the model simple, yet biologically relevant and capable of meaningful predictions. To that end, the developed model contains biologically reasonable assumptions, simplifications and generalizations. A more detailed explanation can be found in the *Supplementary Material*.

Acknowledgements

This work was supported by funding from the German Science Foundation (DFG), the Swiss National Science Foundation, by the Science Foundation Ireland under Grant No. 06/CE/B1129, by the Young Scholar Fund of the University of Konstanz and by funding from the Kanton of Thurgau. We thank Isabell Winter for technical assistance on cloning STYX-G120C.

References

1. Keshet Y,Seger R (2010) The MAP Kinase Signaling Cascades: A System of Hundreds of Components Regulates a Diverse Array of Physiological Functions. *MAP Kinase Signaling Protocols,* Methods in Molecular Biology, (Humana Press), Vol 661, pp 3-38.
2. Yoon S,Seger R (2006) The extracellular signal-regulated kinase: Multiple substrates regulate diverse cellular functions. *Growth Factors* 24(1):21-44.
3. Kim Y *et al.* (2011) Substrate-dependent control of MAPK phosphorylation in vivo. *Mol Syst Biol* 7:467.
4. Teis D, Wunderlich W,Huber L-A (2002) Localization of the MP1-MAPK Scaffold Complex to Endosomes Is Mediated by p14 and Required for Signal Transduction. *Dev Cell* 3(6):803-814.
5. Torii S, Kusakabe M, Yamamoto T, Maekawa M,Nishida E (2004) Sef Is a Spatial Regulator for Ras/MAP Kinase Signaling. *Dev Cell* 7(1):33-44.
6. Blüthgen N *et al.* (2009) A systems biological approach suggests that transcriptional feedback regulation by dual-specificity phosphatase 6 shapes extracellular signal-related kinase activity in RAS-transformed fibroblasts. *FEBS J* 276(4):1024.
7. Wishart M-J, Denu J-M, Williams J-A,Dixon J-E (1995) A Single Mutation Converts a Novel Phosphotyrosine Binding Domain into a Dual-specificity Phosphatase. *J Biol Chem* 270(45):26782-26785.
8. Wishart M-J,Dixon J-E (2002) The archetype STYX/dead-phosphatase complexes with a spermatid mRNA-binding protein and is essential for normal sperm production. *Proc Natl Acad Sci USA* 99(4):2112-2117.
9. Maiwald T,Timmer J (2008) Dynamical modeling and multi-experiment fitting with PottersWheel. *Bioinformatics* 24(18):2037-2043.
10. Brunner D *et al.* (1994) A gain-of-function mutation in Drosophila MAP kinase activates multiple receptor tyrosine kinase signaling pathways. *Cell* 76(5):875-888.
11. Tanoue T, Adachi M, Moriguchi T,Nishida E (2000) A conserved docking motif in MAP kinases common to substrates, activators and regulators. *Nat Cell Biol* 2(2):110-116.
12. Dimitri C-A, Dowdle W, MacKeigan J-P, Blenis J,Murphy L-O (2005) Spatially Separate Docking Sites on ERK2 Regulate Distinct Signaling Events In Vivo. *Current biology: CB* 15(14):1319-1324.
13. Caunt C-J, Armstrong S-P, Rivers C-A, Norman M-R,McArdle C-A (2008)

Spatiotemporal Regulation of ERK2 by Dual Specificity Phosphatases. *J Biol Chem* 283(39):26612-26623.

14. Owens D-M,Keyse S-M (2007) Differential regulation of MAP kinase signalling by dual-specificity protein phosphatases. *Oncogene* 26(22):3203-3113.
15. Bisel B *et al.* (2008) ERK regulates Golgi and centrosome orientation towards the leading edge through GRASP65. *J Cell Biol* 182(5):837-843.
16. Yadav S, Puri S,Linstedt A-D (2009) A Primary Role for Golgi Positioning in Directed Secretion, Cell Polarity, and Wound Healing. *Mol Biol Cell* 20(6):1728-1736.
17. Farhan H *et al.* (2010) MAPK signaling to the early secretory pathway revealed by kinase/phosphatase functional screening. *J Cell Biol* 189(6):997-1011.
18. Marshall C-J (1995) Specificity of receptor tyrosine kinase signaling: Transient versus sustained extracellular signal-regulated kinase activation. *Cell* 80(2):179-185.
19. Vaudry D, Stork P-J-S, Lazarovici P,Eiden L-E (2002) Signaling Pathways for PC12 Cell Differentiation: Making the Right Connections. *Science* 296(5573):1648-1649.
20. von Kriegsheim A *et al.* (2009) Cell fate decisions are specified by the dynamic ERK interactome. *Nat Cell Biol* 11(12):1458-1464.
21. Chaffer C-L,Weinberg R-A (2011) A Perspective on Cancer Cell Metastasis. *Science* 331(6024):1559-1564.
22. Mandl M, Slack D-N,Keyse S-M (2005) Specific Inactivation and Nuclear Anchoring of Extracellular Signal-Regulated Kinase 2 by the Inducible Dual-Specificity Protein Phosphatase DUSP5. *Mol Cell Biol* 25(5):1830-1845.
23. Casar B, Rodríguez J, Gibor G, Seger R,Crespo P (2012) Mxi2 sustains ERK1/2 phosphorylation in the nucleus by preventing ERK1/2 binding to phosphatases. *Biochem J* 441(2):571-578.
24. Casar B *et al.* (2007) Mxi2 promotes stimulus-independent ERK nuclear translocation. *EMBO J* 26(3):635.
25. Tang D, Yuan H,Wang Y (2010) The Role of GRASP65 in Golgi Cisternal Stacking and Cell Cycle Progression. *Traffic* 11(6):827.
26. Shaul Y-D,Seger R (2006) ERK1c regulates Golgi fragmentation during mitosis. *J Cell Biol* 172(6):885-897.
27. Ekerot M *et al.* (2008) Negative-feedback regulation of FGF signalling by DUSP6/MKP-3 is driven by ERK1/2 and mediated by Ets factor binding to a conserved site within the DUSP6/MKP-3 gene promoter. *Biochem J* 412(2):287.
28. Chia J *et al.* (2012) RNAi screening reveals a large signaling network controlling the

Golgi apparatus in human cells. *Mol Syst Biol* 8:629.

29. Gröschl B *et al.* (2011) Expression of the MAP kinase phosphatase DUSP4 is associated with microsatellite instability in colorectal cancer (CRC) and causes increased cell proliferation. *Int J Cancer* [Epub ahead of print].
30. Balko J-M *et al.* (2012) Profiling of residual breast cancers after neoadjuvant chemotherapy identifies DUSP4 deficiency as a mechanism of drug resistance. *Nat Med* 18(7):1052-1059.
31. Chen J-Y, Lin J-R, Cimprich K-A,Meyer T (2012) A Two-Dimensional ERK-AKT Signaling Code for an NGF-Triggered Cell-Fate Decision. *Mol Cell* 45(2):196.
32. Zhao Y,Zhang Z-Y (2001) The Mechanism of Dephosphorylation of Extracellular Signal-regulated Kinase 2 by Mitogen-activated Protein Kinase Phosphatase 3. *J Biol Chem* 276(34):32382-32391.
33. Ferrell J-E,Bhatt R-R (1997) Mechanistic Studies of the Dual Phosphorylation of Mitogen-activated Protein Kinase. *J Biol Chem* 272(30):19008-19016.
34. Burack W-R,Sturgill T-W (1997) The Activating Dual Phosphorylation of MAPK by MEK Is Nonprocessive. *Biochemistry* 36(20):5929-5933.
35. Fujioka A *et al.* (2006) Dynamics of the Ras/ERK MAPK Cascade as Monitored by Fluorescent Probes. *J Biol Chem* 281(13):8917-8926.
36. Nakakuki T *et al.* (2010) Ligand-Specific c-Fos Expression Emerges from the Spatiotemporal Control of ErbB Network Dynamics. *Cell* 141(5):884-896.
37. Kucharska A, Rushworth L-K, Staples C, Morrice N-A,Keyse S-M (2009) Regulation of the inducible nuclear dual-specificity phosphatase DUSP5 by ERK MAPK. *Cell Signal* 21(12):1794-1805.
38. Legewie S, Herzel H, Westerhoff H-V,Bluthgen N (2008) Recurrent design patterns in the feedback regulation of the mammalian signalling network. *Mol Syst Biol* 4:190.

Figure Legends

Figure 1. Localization of STYX and modeling its possible modes of action. *A,* schematic illustration of the hypothetical modes of action of STYX (left panel) and the corresponding predictions of the cellular ppERK activation dynamics (right panel) in control (solid blue line)

and STYX-depleted (dashed green line) conditions. *B,* Localization of overexpressed YFP-tagged STYX in serum-starved (strv) and serum-stimulated (stim) cells. The right panel shows HeLa cells expressing YFP alone. Staining of the nucleus was achieved using Alexa Fluor647-Toto3 (red). *C,* Localization of endogenous STYX (green) in HeLa cells in serum-starved (Strv) and serum-stimulated (stim) cells. Staining of the nucleus was achieved using Alexafluor647-Toto3 (red). Scale bar= 10 µm. *D,* HeLa cells were transfected with plasmids encoding HA-tag, HA-tagged wild type STYX (HA-STYX-wt) or STYX-G120C (HA-STYX-G120C). After 24 h, cells were lysed and STYX was immunoprecipitated using anti-HA coupled sepharose beads. Immunoprecipitate was washed and incubated with recombinant ppERK2 for 30 min followed by SDS-PAGE and immunoblotting against the indicated proteins.

Figure 2. Testing model predictions experimentally. Knockdown of STYX increases ppERK. *A,* HeLa cells were transfected with non-targeting siRNA oligos (control) or with siRNA against STYX (STYX knockdown). After 72 h, cells were serum starved followed by stimulation with 10% FCS for the indicated time points, then lysed and the indicated proteins were detected by immunoblotting. Lower panel shows a representative experiment and the right panel a densitometric evaluation of three independent experiments. *B,* Model predictions of the cytosolic and nuclear ppERK activation dynamics in control (solid blue line) and STYX knockdown conditions (dashed green line). *C&D,* HeLa cells were transfected as described in panel A and samples were immunoblotted to detect levels of phosphorylated RSK (pRSK, panel C) and phosphorylated Elk1 (pElk, panel D). Tubulin and GM130 were detected to ensure equal gel loading. *E,* HeLa cells were transfected with plasmids encoding YFP1-tagged ERK2 and YFP2-tagged STYX. After 24 h, cells were fixed and images were acquired using a confocal laser scanning microscope. Scale bar = 10 µm. *F,* in vitro translated YFP2-tagged STYX (YFP2-STYX) or YFP2 alone was immunoprecipitated with an anti-GFP

antibody that recognizes the C-terminal portion of YFP (i.e. YFP2). The washed immunoprecipitate was then incubated with purified GST-tagged ERK2 followed by washing and loading of the samples on a SDS-polyacrylamide gel and immunoblotted against the indicated proteins. *G,* HeLa were co-transfected with plasmids encoding flag-tagged ERK2 together with YFP (no STYX) or together with YFP-tagged STYX. Cells co-expressing YFP-STAY and flag-ERK2 were either grown under steady state conditions (SS), or were serum-starved (strv), or were serum-starved and then stimulated by 10% FCS for 15 min (stim). Cells were lysed and the lysate was immunoprecipitated against flag followed by immunoblotting against the indicated proteins.

Figure 3. Calibration of model 1 and validating refined predictions. *A,* Fit of the calibrated model to the training data. To quantitatively test model 1, it was fitted to the ppERK time-course data and to obtain several good-fitting parameter sets for further analysis, the optimization algorithm (adaptive simulated annealing) was started several times (n>30); thin lines are simulated trajectories of the individual fits in control and STYX knockdown conditions, thick lines represent the corresponding mean. Dots and error-bars indicate the mean and standard deviation of the training data set. *B,* Estimated parameter values (dots) of the total STYX concentration and the STYX-ERK dissociation constant and their correlation (regression line). *C,* Model prediction of the STYX overexpression time-course in comparison to the experimental validation data set. Thin lines indicate the individual predictions using the each estimated parameter set, bold lines the mean (n>30). *D,* Validation experiment. HeLa cells were transfected with empty vector (control) or with a cDNA encoding HA-tagged STYX (HA-STYX). After 24 h, cells were serum-starved followed by stimulation with 10% FCS for the indicated time points. Cells were lysed and lysates were subjected to immunoblotting against the indicated proteins.

Figure 4. STYX acts as a nuclear anchor for ERK. *A,* HeLa cells were transfected with non-targeting siRNA oligos (control) or with siRNA targeting STYX. After 72 h nuclear and cytosolic fractions were prepared as described in "*Materials and Methods*". The fractions were loaded on SDS-polyacrylamide gels followed by immunoblotting against the indicated proteins. *B,* Predictions of the ERK nuclear efflux rates by model 1. Thin lines are the individual predictions generated by the estimated parameter sets (n>30) for control (red) and STYX k.d. (blue) conditions with the dotted and dashed bold line indicating the respective mean. *C,* Validation experiments measuring ERK nuclear efflux. For knockdown experiments, HeLa cells were transfected with the non targeting siRNA oligos (siCont) or with siRNA against STYX (siSTYX). After 48 h, cells were transfected with a plasmid encoding GFP-tagged ERK2. For overexpression experiments HeLa cells were transfected with cDNA encoding GFP-ERK2 together with either empty vector (HA overexp) or with a plasmid encoding HA-tagged STYX (STYX overexp). FRAP experiments were performed as described in "*Materials and Methods*". The left panel shows two representative images series of FRAP experiments from knockdown experiments. Cells displayed were acquired before photobleaching (Pre), directly after photobleaching the cytosol (Post) and at the end of the recovery phase (Rec). Right panel shows an evaluation of fluorescence recoveries plotted as an increase of fluorescence intensity as fold of the post-bleach value.

Figure 5. STYX and DUSP4 compete for binding to ERK. *A,* HeLa cells in 10 cm cell culture dishes were transfected with plasmids encoding flag-ERK2 and YFP-STYX together with either empty vector (no DUSP4), or with 3 μg DUSP4 (low DUSP4), or with 5.4 μg DUSP4 (high DUSP4). Cells were lysed and the lysates were subjected to immunoprecipitation against flag (ERK2) and immunoblotted against indicated proteins. IN= 3% input to the immunoprecipitation (IP). *B,* HeLa cells were transfected with a combination of YFP1-tagged

ERK2 (Y1-ERK2) and YFP2-tagged STYX (Y2-STYX) together with increasing amounts (0.5, 1 and 1.5 μg) of DUSP4 expression plasmid. Cells were fixed after 16 h and the YFP-fluorescence was recorded using a confocal laser scanning microscope. Lower panel shows representative cells and upper panel an evaluation of fluorescence intensities measured from three experiments. *C,* HeLa cells were transfected with YFP-tagged STYX or myc-tagged DUSP4 together with either flag-tagged wild type ERK2 (wt) or flag-tagged mutant ERK2 (D319N). After 24 h, cells were lysed and the lysate was subjected to immunoprecipitation against flag-tagged ERK variants. The amount of co-immunoprecipitated STYX or DUSP4 was detected by immunoblotting. IN= 3 % input to the immunoprecipitation (IP).

Figure 6. STYX regulates Golgi structure and directional cell migration. *A,* HeLa cells were transfected with non-targeting siRNA oligos (Cont) or with siRNA targeting STYX (siSTYX). After 48 h, cells were treated with solvent or with PD98059 (+PD) for 18 h followed by fixation in paraformaldehyde. Golgi was stained by immunofluorescence against GM130. Shown are representative images from each condition. White boxes indicate cells that were magnified. In order to facilitate appreciation of the Golgi phenotype a mask of the Golgi is displayed next to each magnified image. The lowest panel shows an evaluation of the percentage of cells that display a fragmented Golgi from three experiments with a minimum of 100 cells that were counted in each experiment. *B&C,* HeLa cells were transfected with non-targeting siRNA oligos (Cont) or with siRNA targeting STYX (siSTYX). After 48 h, cells were transferred to ibidi® chambers that generates a "wound" of 600 μm width. After 8 h, migration was initiated by removal of the chamber and cells were fixed after 20 h and stained against GM130 to visualize the Golgi. To visualize the extent of cell migration, images were acquired with a 10x objective (B) and to visualize orientation of the Golgi images were acquired using the 63x objective (C). Black line in panel B indicates the two wound edges. White line in panel C indicates the position of the leading edge. The width of the wound was

measured (B) and the amount of cells with a Golgi facing the wound were counted (C) and the results are displayed in the bar graphs on the right side of the panels.

Figure 7. STYX regulates cell fate decisions. *A,* PC12 cells plated on collagen coated cover slips were transfected with plasmids encoding YFP alone of YFP-tagged STYX (YFP-STYX). After 24 h, cells were either fixed directly (t0) or treated with NGF for 60 min (t60) followed by fixation. ppERK was visualized using immunofluorescence staining. Arrows indicate the position of YFP-expressing cells. *B,* PC12 cells plated on collagen coated cover slips were transfected with plasmids encoding YFP alone of YFP-tagged STYX (YFP-STYX). After 24 h, serum was reduced to 1% horse serum and cells were treated with NGF for 24 and 48 h, followed by fixation and confocal imaging. The amount of differentiated, YFP-positive PC12 cells was assessed as described in "*Materials and Methods*".

A

Model 1

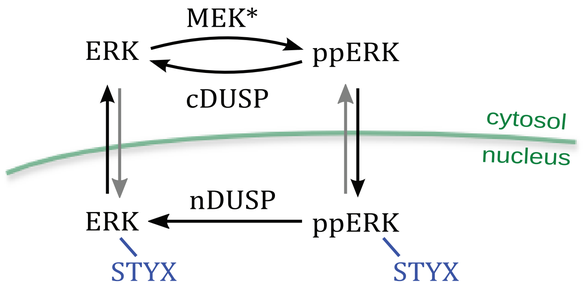

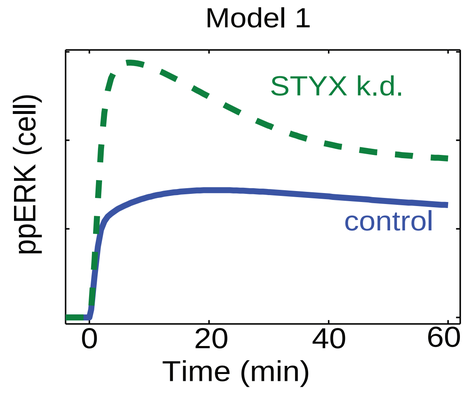

Model 2

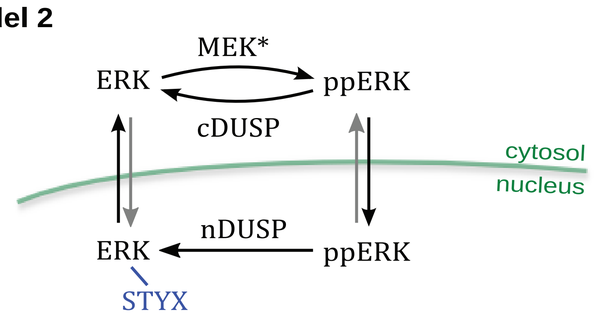

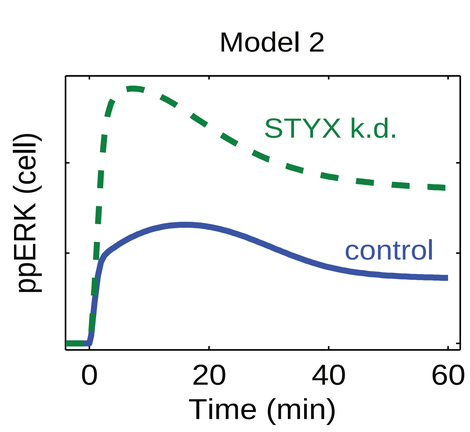

Model 3

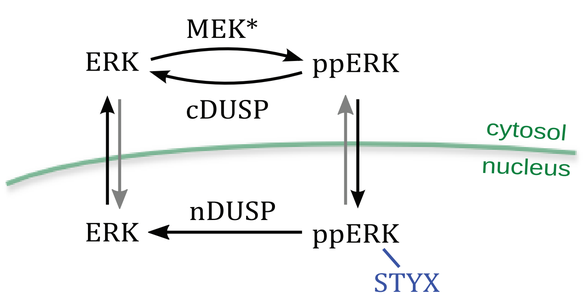

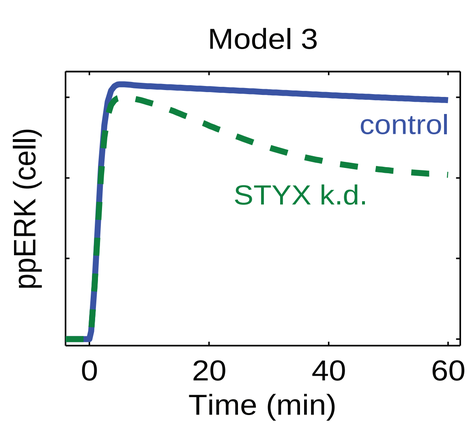

Model 4

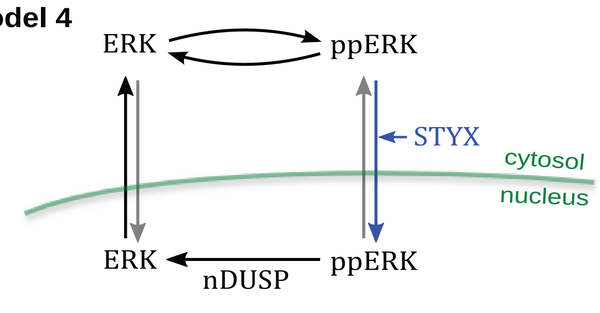

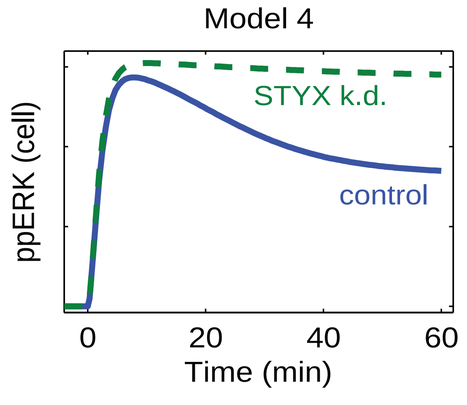

Model 5

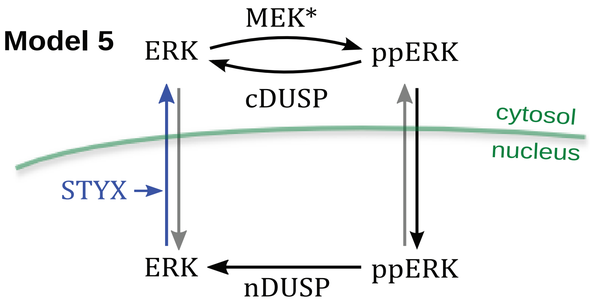

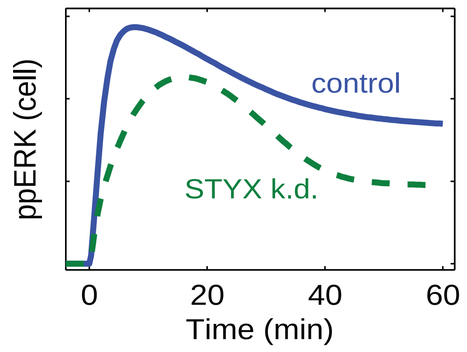

B

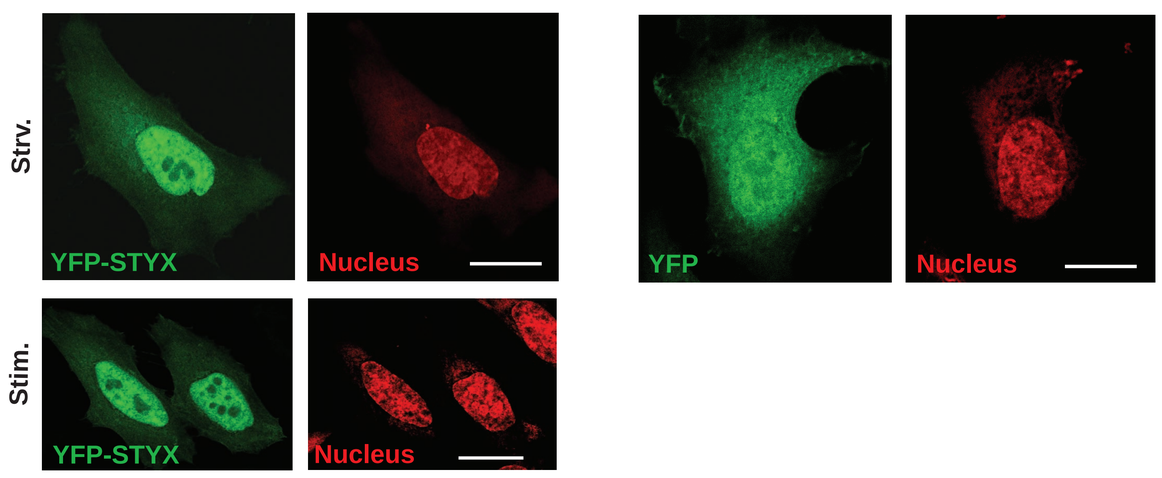

C

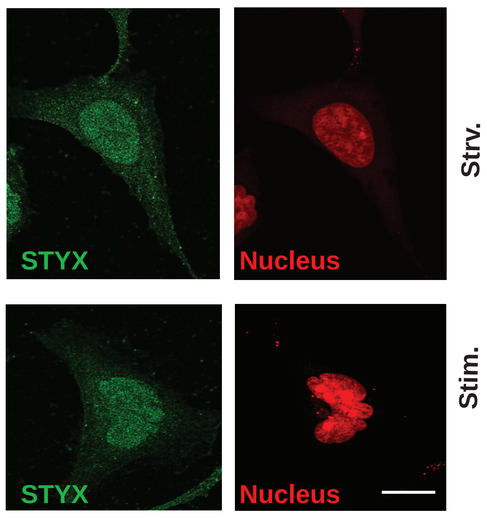

D

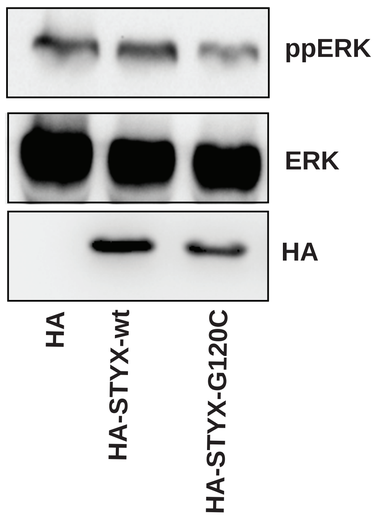

A

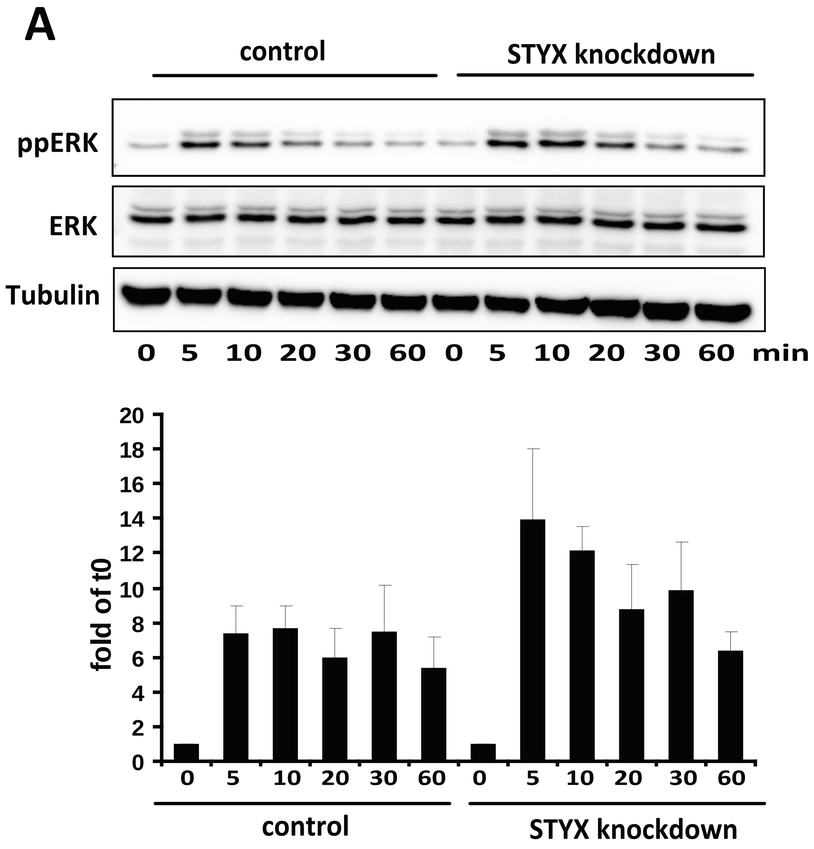
control
STYX knockdown
ppERK
ERK
Tubulin
0 5 10 20 30 60 0 5 10 20 30 60 min
fold of t0
0 5 10 20 30 60 0 5 10 20 30 60
control
STYX knockdown

B

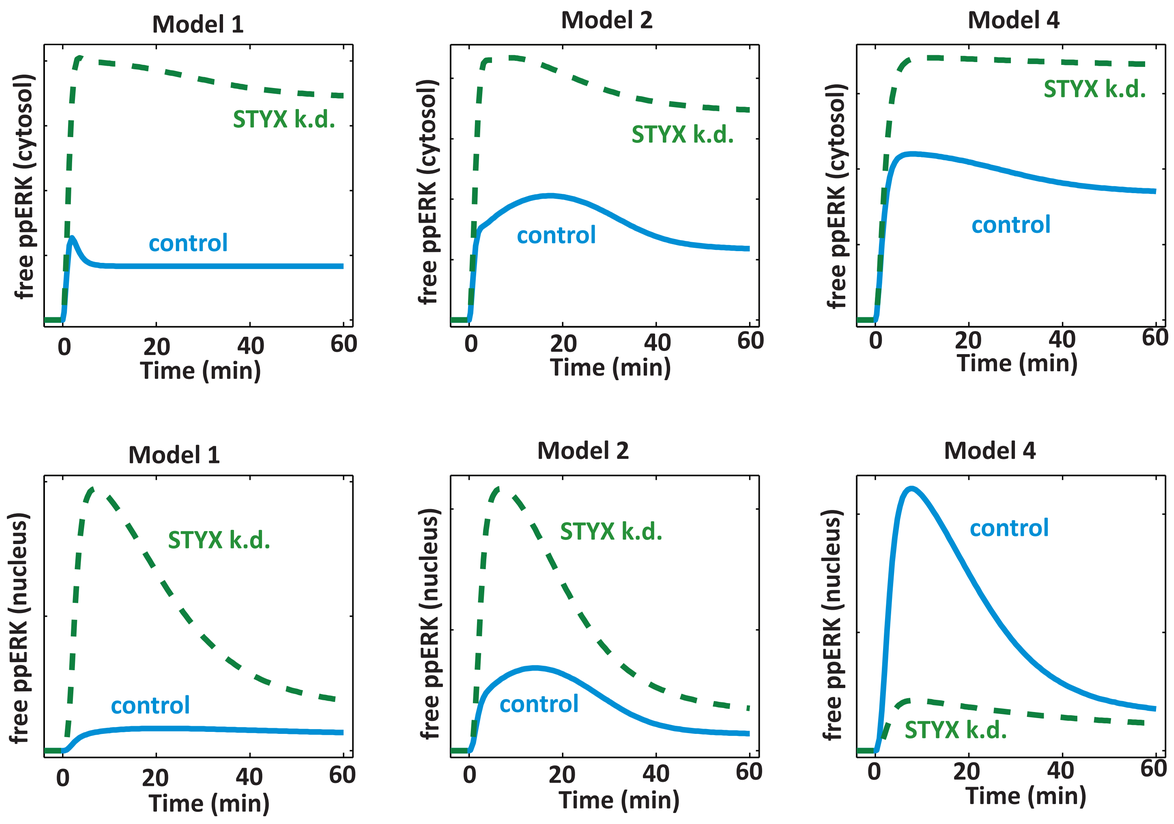
Model 1
Model 2
Model 4
free ppERK (cytosol)
free ppERK (nucleus)
STYX k.d.
control
Time (min)

C

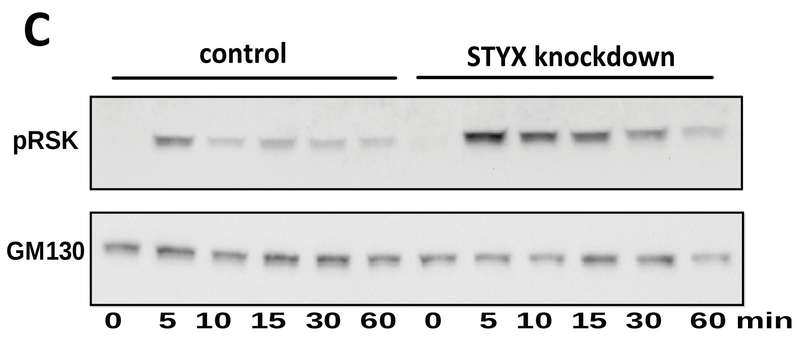
control
STYX knockdown
pRSK
GM130
0 5 10 15 30 60 0 5 10 15 30 60 min

D

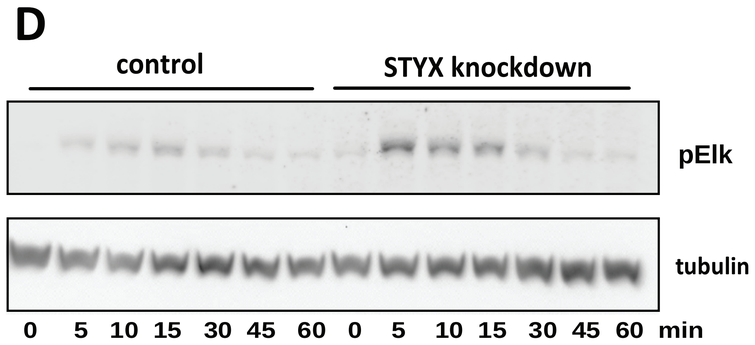
control
STYX knockdown
pElk
tubulin
0 5 10 15 30 45 60 0 5 10 15 30 45 60 min

E

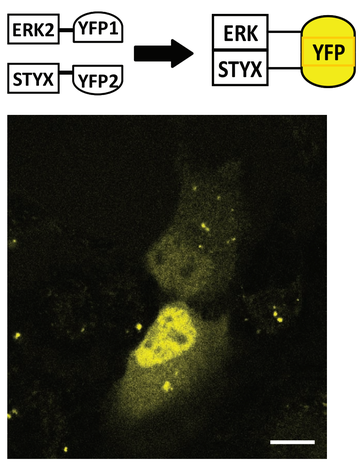
ERK2
YFP1
STYX
YFP2
ERK
STYX
YFP

F

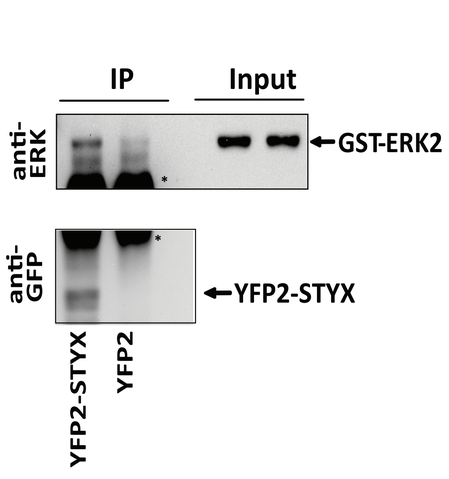
IP
Input
anti-ERK
GST-ERK2
anti-GFP
YFP2-STYX
YFP2-STYX
YFP2

G

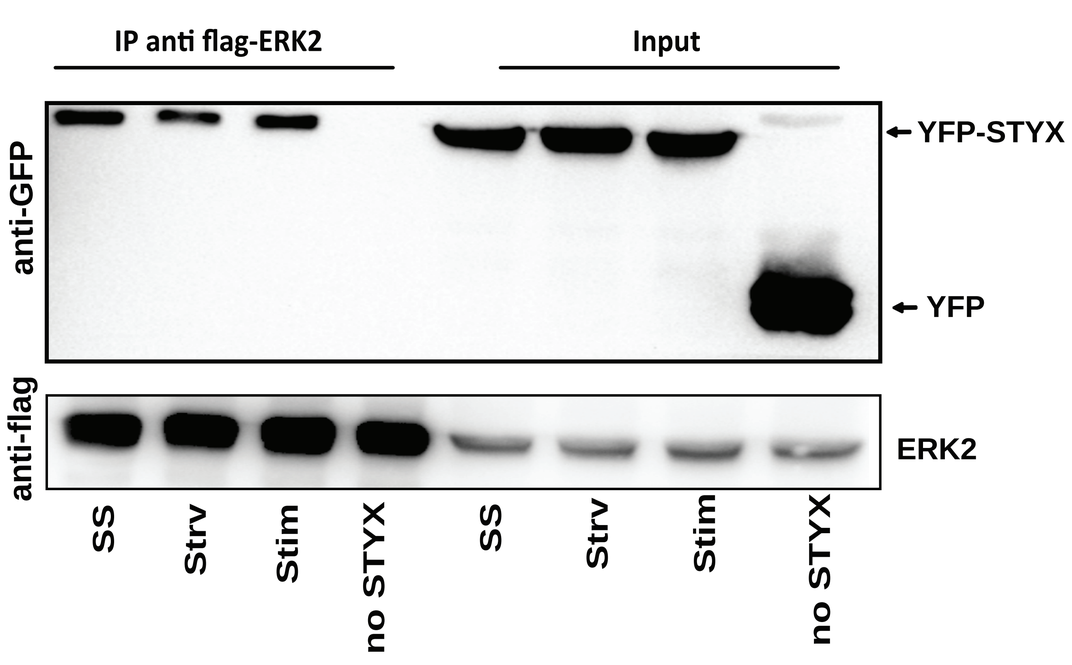
IP anti flag-ERK2
Input
anti-GFP
YFP-STYX
YFP
anti-flag
ERK2
SS
Strv
Stim
no STYX

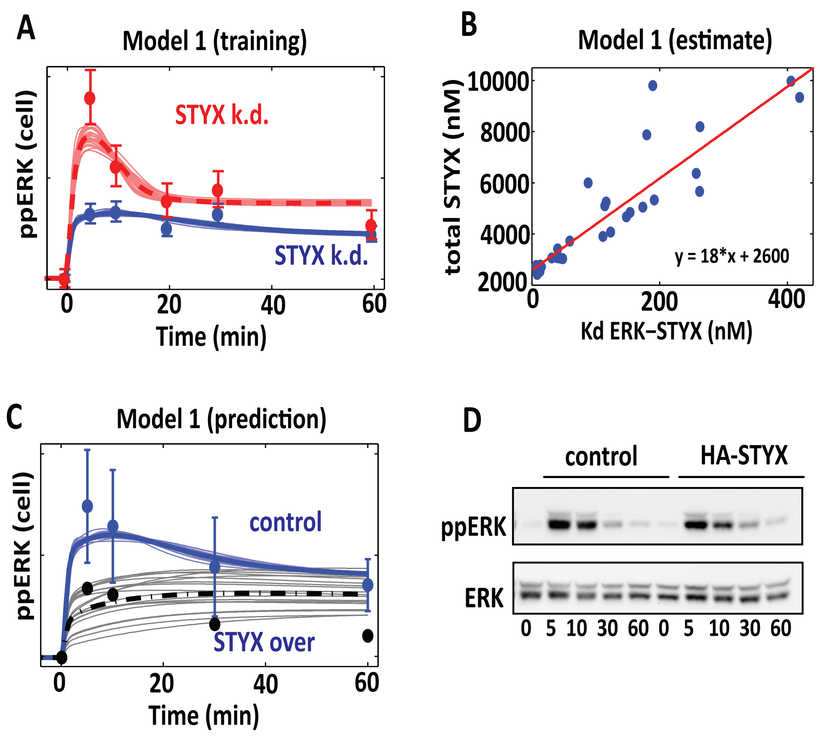
A
Model 1 (training)
ppERK (cell)
STYX k.d.
STYX k.d.
0
20
40
60
Time (min)
B
Model 1 (estimate)
total STYX (nM)
10000
8000
6000
4000
2000
y = 18*x + 2600
0
200
400
Kd ERK–STYX (nM)
C
Model 1 (prediction)
ppERK (cell)
control
STYX over
0
20
40
60
Time (min)
D
control
HA-STYX
ppERK
ERK
0 5 10 30 60 0 5 10 30 60

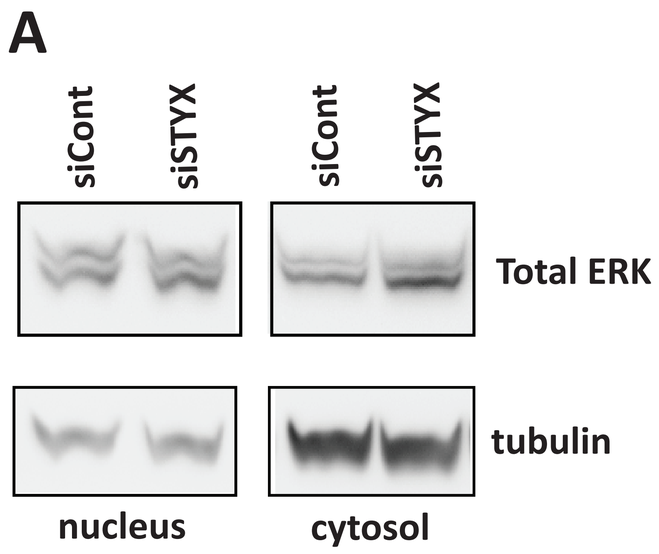
A
siCont
siSTYX
siCont
siSTYX
Total ERK
tubulin
nucleus
cytosol

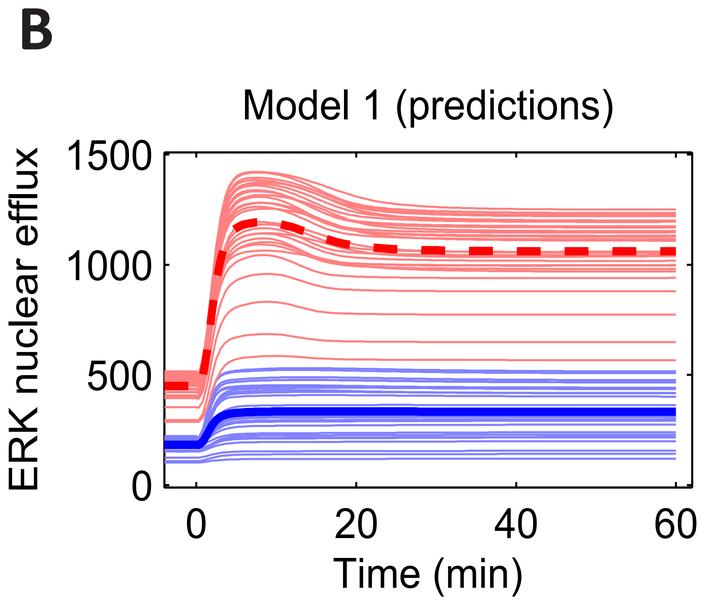
B
Model 1 (predictions)
ERK nuclear efflux
1500
1000
500
0
0
20
40
60
Time (min)

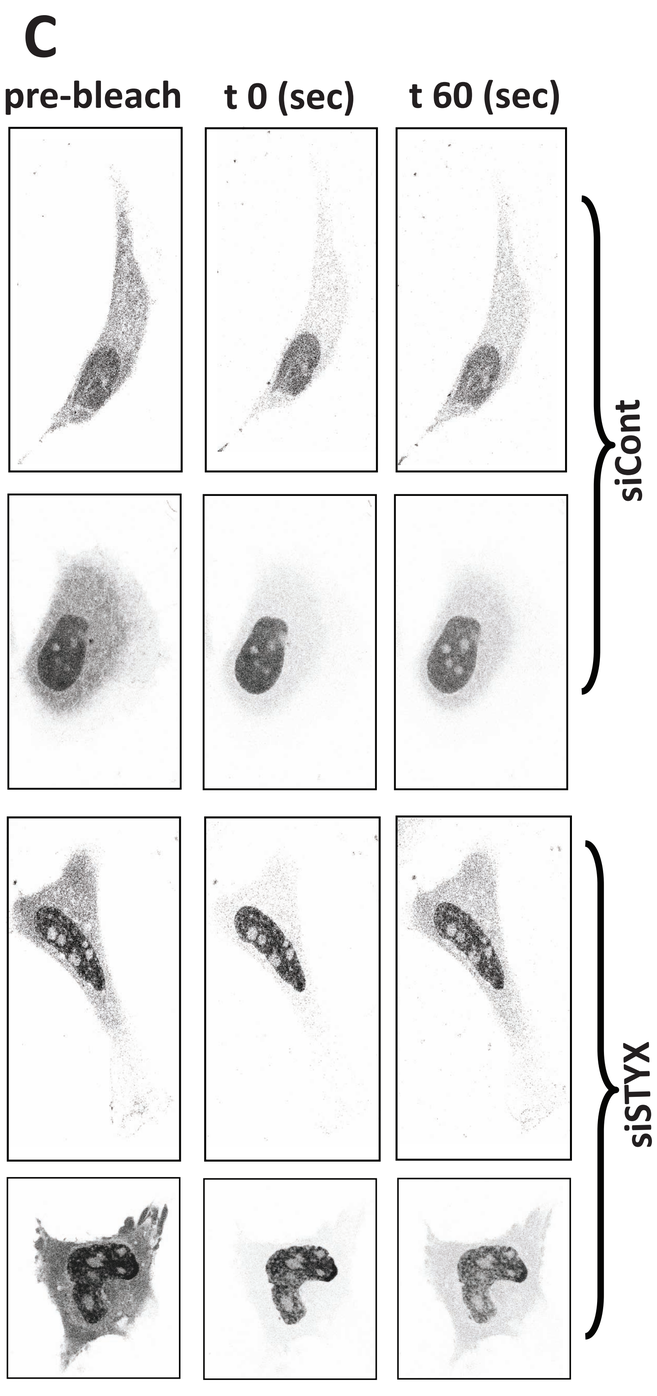
C
pre-bleach
t 0 (sec)
t 60 (sec)
siCont
siSTYX

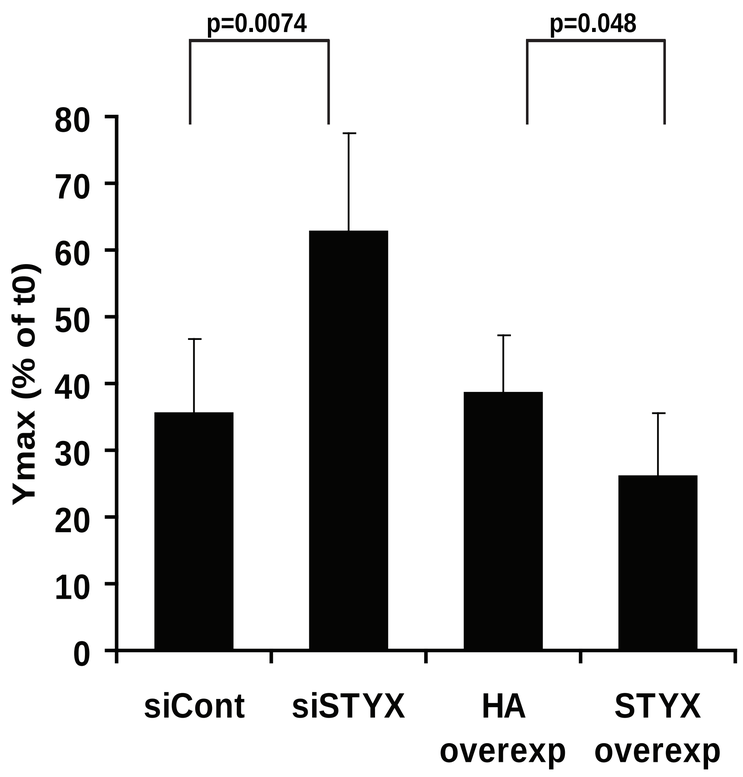
p=0.0074
p=0.048
Ymax (% of t0)
80
70
60
50
40
30
20
10
0
siCont
siSTYX
HA
overexp
STYX
overexp

A

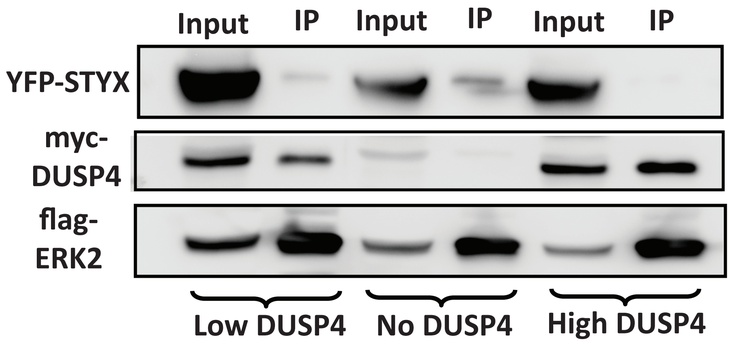
Input
IP
Input
IP
Input
IP
YFP-STYX
myc-DUSP4
flag-ERK2
Low DUSP4
No DUSP4
High DUSP4

B

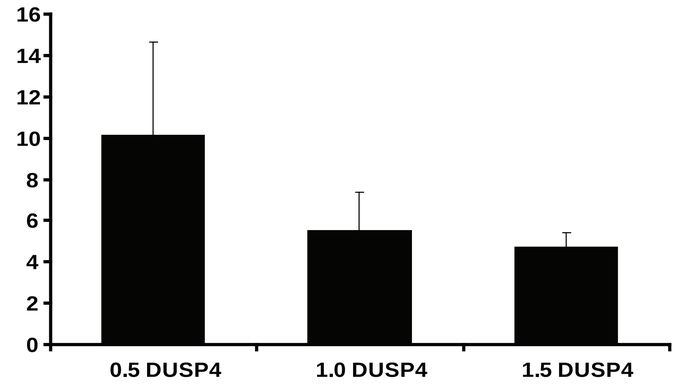
16
14
12
10
8
6
4
2
0
0.5 DUSP4
1.0 DUSP4
1.5 DUSP4

C

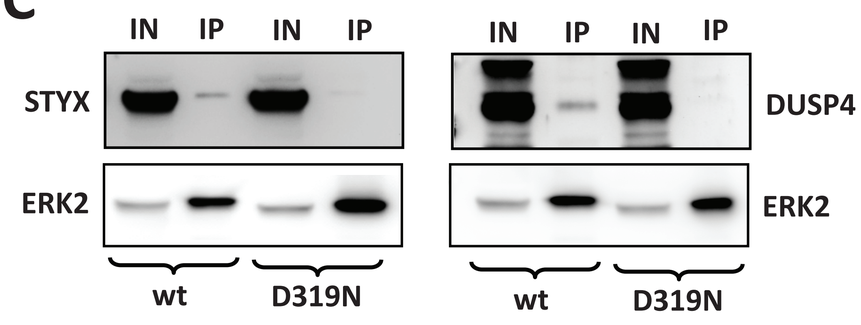
IN
IP
IN
IP
IN
IP
IN
IP
STYX
DUSP4
ERK2
ERK2
wt
D319N
wt
D319N

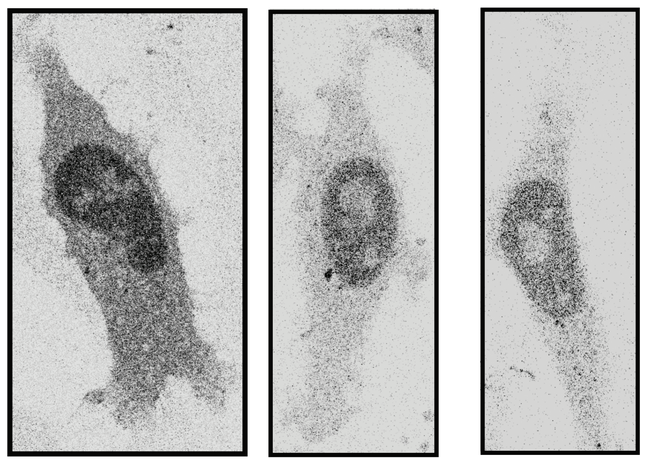

A

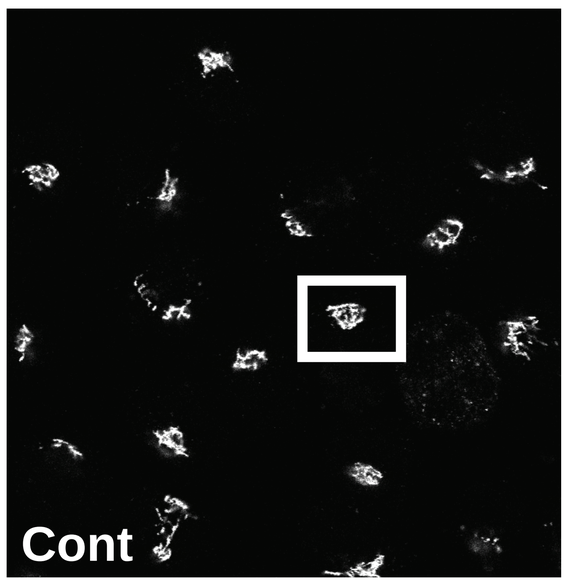
Cont

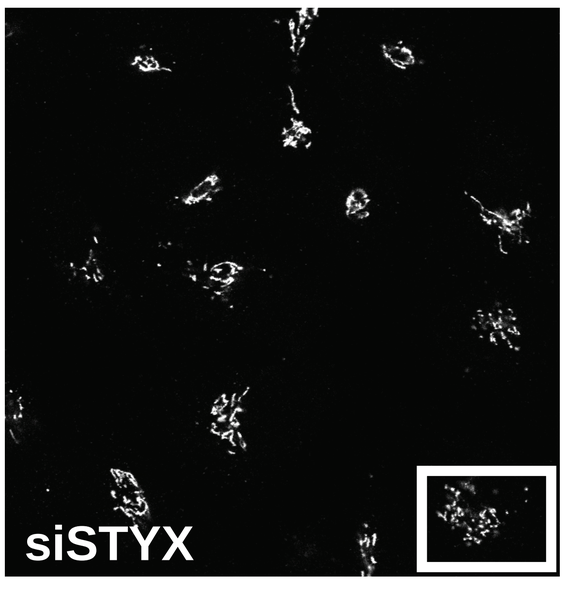
siSTYX

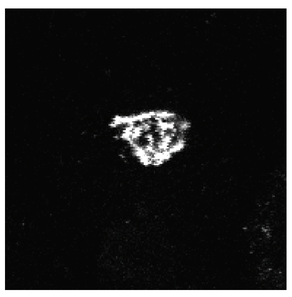

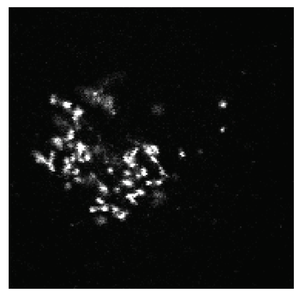

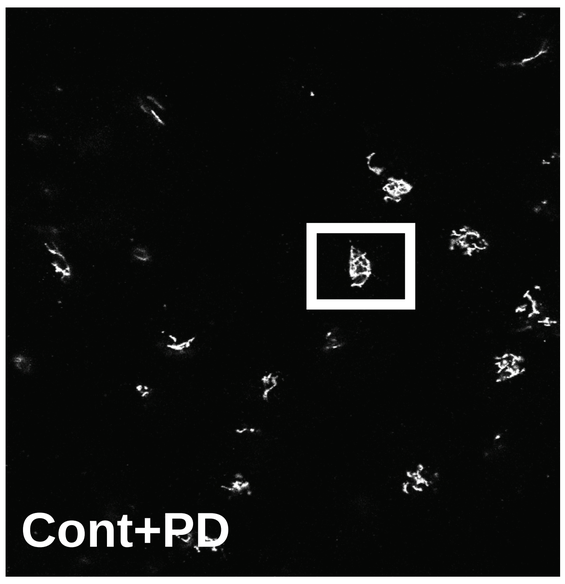
Cont+PD

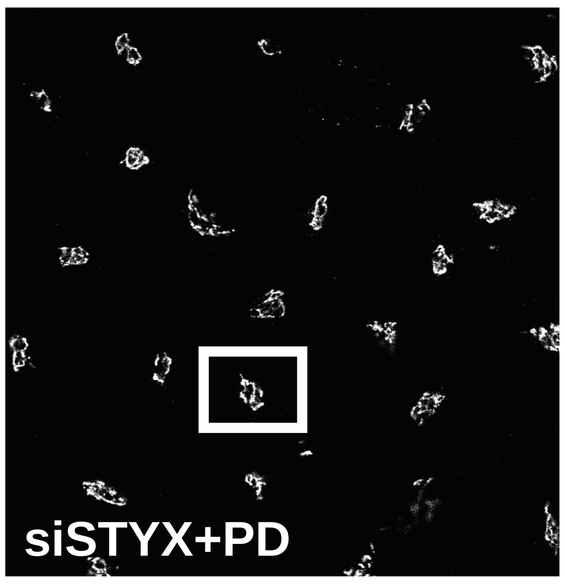
siSTYX+PD

fragmented Golgi (%)
40.0
35.0
30.0
25.0
20.0
15.0
10.0
5.0
0.0
Cont
siSTYX
Cont+PD
siSTYX+PD

B

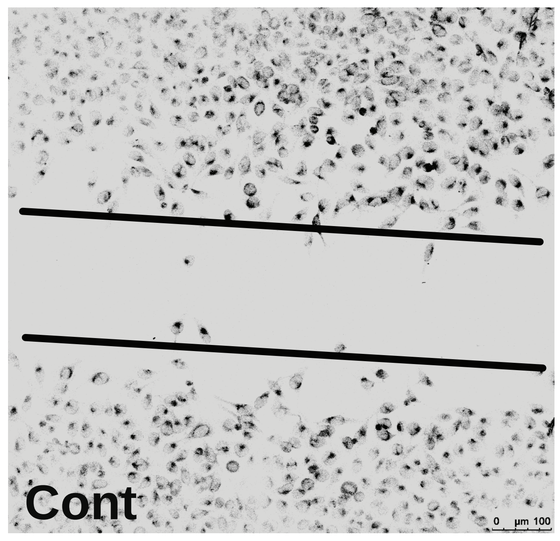
Cont
0 μm 100

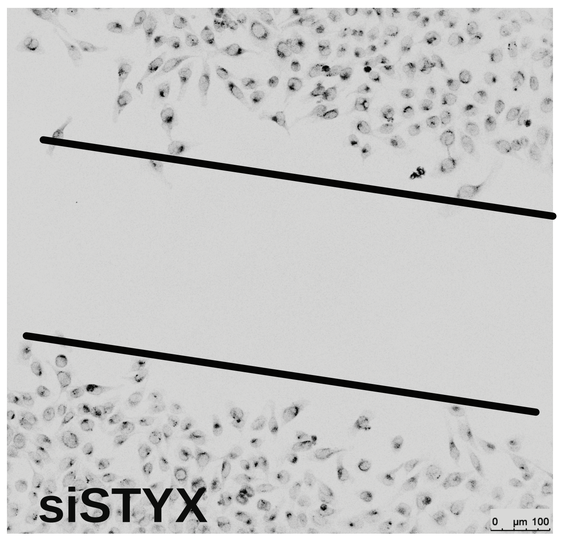
siSTYX
0 μm 100

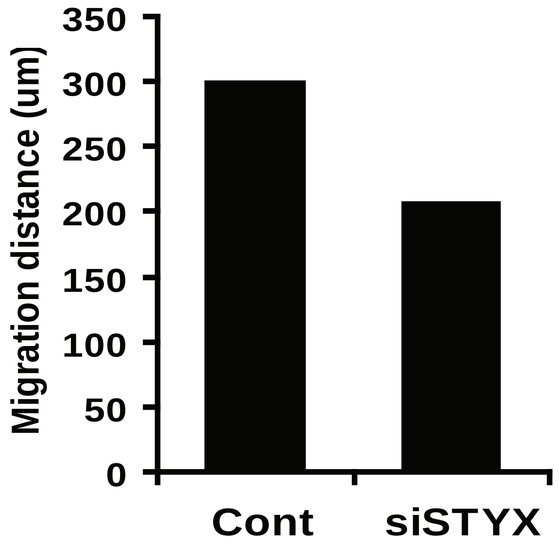
Migration distance (um)
350
300
250
200
150
100
50
0
Cont
siSTYX

C

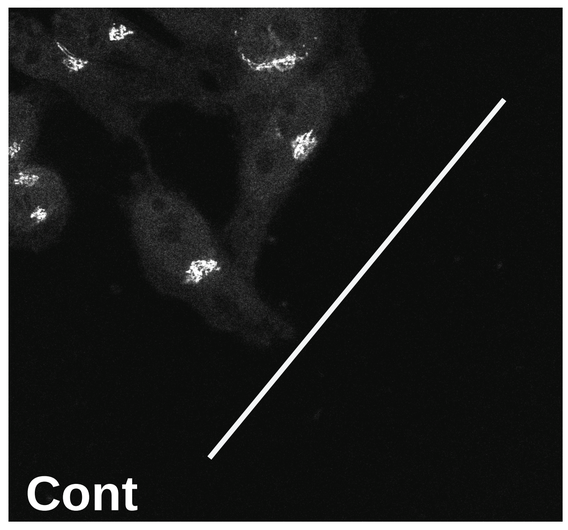
Cont

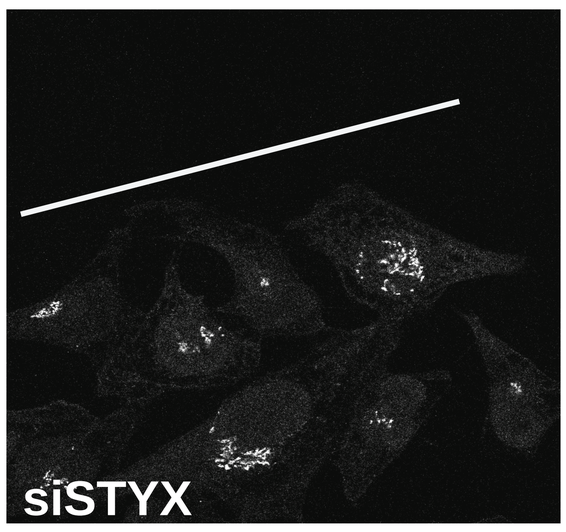
siSTYX

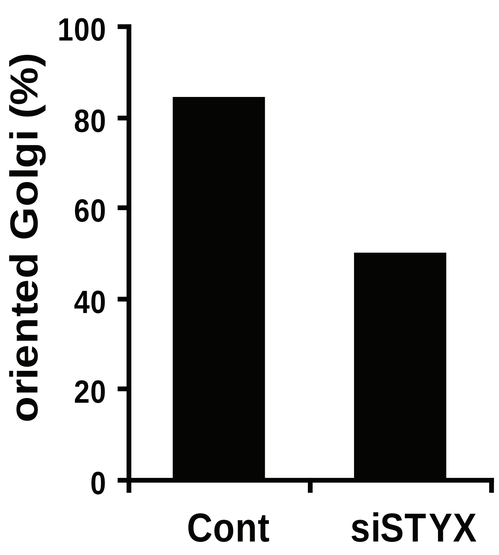
oriented Golgi (%)
100
80
60
40
20
0
Cont
siSTYX

A

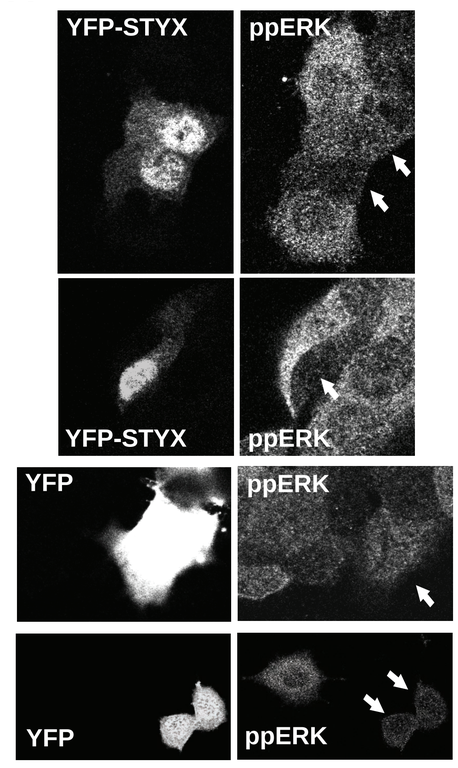
YFP-STYX
ppERK
YFP-STYX
ppERK
YFP
ppERK
YFP
ppERK

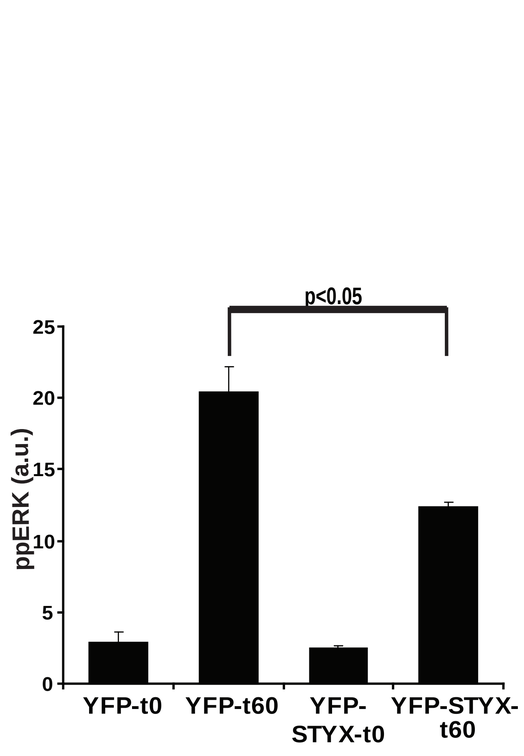
p<0.05
ppERK (a.u.)
25
20
15
10
5
0
YFP-t0
YFP-t60
YFP-STYX-t0
YFP-STYX-t60

B

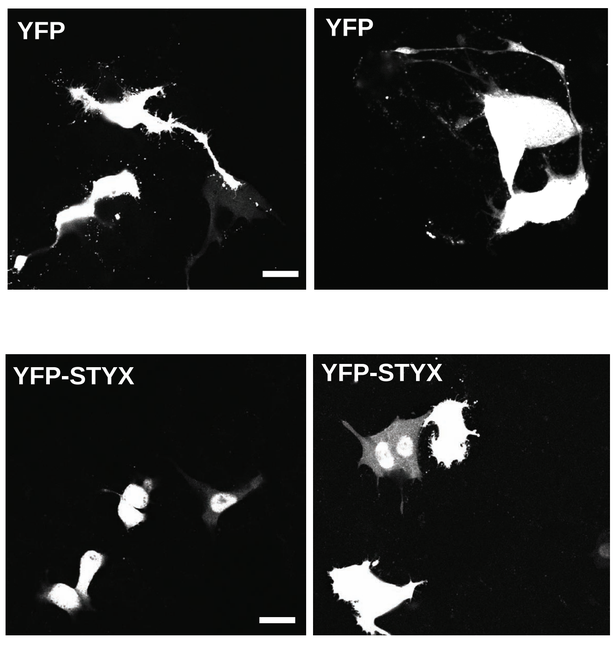
YFP
YFP
YFP-STYX
YFP-STYX

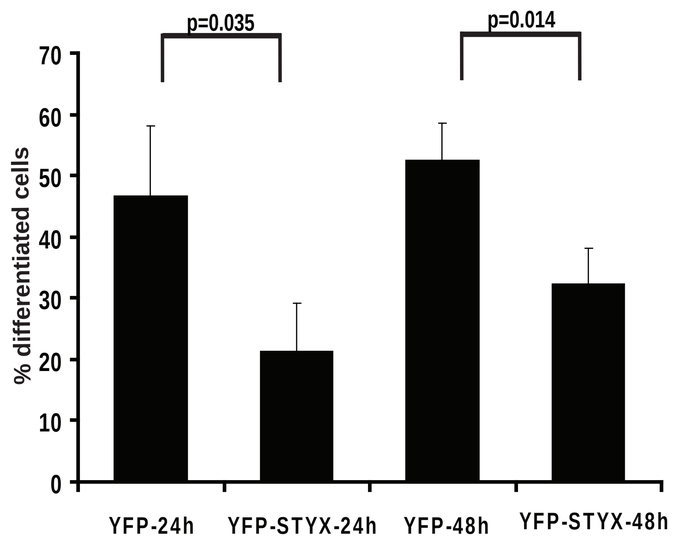
p=0.035
p=0.014
% differentiated cells
70
60
50
40
30
20
10
0
YFP-24h
YFP-STYX-24h
YFP-48h
YFP-STYX-48h

Detailed model scheme

Core model of ERK signaling

The common core of our models (Fig. S3A) is based on the established, well calibrated models of ERK signaling. First, active MEK binds ERK in the cytosol and phosphorylates it at two distinct phosphorylation sites in its kinase domain following a distributive two-collision mechanism (1, 2& 3) Second, all differentially phosphorylated forms of ERK can shuttle into and out of the nucleus with the rates given in Tables S1 and S2 (4). Third, cytosolic and nuclear DUSPs bind and dephosphorylate ERK in their respective compartments, whereas the expression of nuclear DUSP is induced by the nuclear ERK activity (5, 6, 7, & 8). A detailed account of all reactions and differential equations in the model is given in Tables S1 and S2. A successful modeling strategy keeps the model simple, yet biologically relevant and capable of meaningful predictions. To that end, the developed model contains biologically reasonable assumptions, simplifications and generalizations, which the following sections explain in detail.

ERK phosphorylation and dephosphorylation

In concordance with earlier models, based on the fact that the ERK1/2 isoforms share the same upstream kinases, phosphatases and downstream regulators (9) and neglecting possible differences in the ERK1 and ERK2 nuclear shuttling rates (10), our model does not distinguish the two ERK isoforms, but features a combined ERK1/2 component. The validity of this simplification is further supported by our observation that the STYX effect is not confined to either ERK1/2 isoform (Fig. S5). In order to extend the core model to include ERK-STYX binding and the potential competition of STYX and DUSP, we model all phosphorylation and dephosphorylation processes by explicitly accounting for the enzyme-substrate complexes leading to schemes of the form

$$A + B \underset{2}{\overset{1}{\rightleftharpoons}} AE \xrightarrow{3} C + E,$$

where A denotes the substrate (e.g. ERK), B the enzyme (e.g. active MEK), AE the enzyme-substrate complex, C the product (e.g. pERK) and the numbers 1,2 & 3 refer to the association, dissociation and catalytic reactions, respectively. Consequently, all reactions are described mathematically using the law of mass action (the usual Michaelis-Menten-like assumptions may lead to large errors when the concentrations of competing substrates and enzymes are comparable) (11). In concordance with earlier models, we used different affinities for DUSP-ppERK and DUSP-pERK binding (7), and assumed the DUSP-ERK binding affinities to be the same in the cytosol and the nucleus. The model by Nakakuki et al. (7) features Michaelis-Menten like kinetics, with the maximal rate parameter V_{max}

= k_{cat} E, thus we calculated the corresponding catalytic rates in our model as $k_{cat} = V_{max}/E$, where E denotes the enzyme concentration; i.e. the concentration of active MEK for ERK phosphorylation and the concentration of cytosolic DUSP for ERK dephosphorylation in the cytosol. (We assumed active MEK = 100nM, active cDUSP = 100nM for these calculations.)

The catalytic rate of ERK dephosphorylation in the nucleus was consistently estimated to be about 30 - 100-fold higher than the corresponding cytosolic rate (7). Based on this information and the assumption that the basal levels of ERK phosphatases in the cytosol and nucleus are comparable, we used k3_ppERKn = 100 k3_ppERKc, k3_ppERKn = 100 k3_ppERKc.

ERK phosphorylation	**k1_ERK** (1/min)	**k2_ERK** (1/min)	**k3_ERK** (1/min)	**k1_pERK** (1/min)	**k2_pERK** (1/min)	**k3_pERK** (1/min)
Cytosol	1	350	13.2	1	350	13.2
Nucleus	-	-	-	-	-	-
ERK dephosphorylation	**kd1_ppERK** (1/min)	**kd2_ppERK** (1/min)	**kd3_ppERK** (1/min)	**kd1_pERK** (1/min)	**kd2_pERK** (1/min)	**kd3_pERK** (1/min)
Cytosol	1	60	0.388	1	160	0.432
Nucleus	1	60	38.8	1	160	43.2

Table S3. Parameter values for ERK phosphorylation and dephosphorylation.

ERK cytosolic-nuclear transport

All differentially phosphorylated forms of ERK can be transported to and from the nucleus following linear kinetics (4), albeit at different rates: non- and mono-phosphorylated ERK prefer the cytosol, whereas double-phosphorylated ERK prefers the nucleus (see 7 and references therein). We assumed equal transport parameters for non- and mono-phosphorylated ERK and adopted the parameter values in Nakakuki et al. (7).

k_ERKin (1/min)	**k_ERKout** (1/min)	**k_pERKin** (1/min)	**k_pERKout** (1/min)	**k_ppERKin** (1/min)	**k_ppERKout** (1/min)
0.144	1.08	0.144	1.08	0.66	0.78

Table S4. Parameter values for ERK cytosolic-nuclear transport.

Phosphatase/DUSP expression

A variety of different phosphatases is capable of dephosphorylating ERK, including the family of dual specificity phosphatases (DUSPs). Different DUSPs might be constitutively expressed or inducible upon ERK activation at different characteristic time-scales (5, 7, & 12). Our model neglects this complexity, but features a cytosolic (cDUSP) and nuclear (nDUSP) components to describe the combined ERK phosphatase activity in the respective compartment. In concordance with Nakakuki et

al. (7), the level of cytosolic DUSP is assumed constant, whereas the nuclear DUSP expression is induced by active ppERK as follows

$$\frac{\mathrm{T_{duspn}}}{\log(2)}\frac{d\,ndusp}{dt} = duspn_{basal}\left(1 + duspn_{ind}\frac{ppERKn^2}{Kdusp^2+ppERKn^2}\right) - ndusp,$$

$$\frac{\mathrm{T_{DUSPn}}}{\log(2)}\frac{d\,nDUSP}{dt} = v_2\,ndusp - nDUSP,$$

where ndusp and nDUSP denote mRNA and protein levels, respectively, T_{duspn} and T_{DUSPn} the corresponding half-lives, $dusp_{basal}$ the level of constitutive expression, $dusp_{ind}$ the corresponding maximal fold-change upon ERK activation and v_2 the translation rate. Because these parameters were uncertain, they were estimated using our own data as described below.

Parameterisation of the model

Most of the parameters in this core model were based on reported measurements of ERK-DUSP interactions, DUSP catalytic activity and ERK cytosolic-nuclear shuttling (see sections above and Markevich et al. (11), Nakakuki et al. (7) and references therein). The remaining unknown parameters relating to DUSP mRNA and protein expression and ERK-STYX binding were estimated based on our own experiments as explained below.

Estimated parameters

Both, the STYX binding parameters and the DUSP expression parameters were uncertain with little or no kinetic information available in the literature. Thus, we estimated these parameters based on the experimentally measured ppERK time-courses in control and STYX knock-down conditions. Some kinetic information was available for DUSPs. For example, DUSP6 exhibits half-lives between 8 min to 40 min on the mRNA level and the half-life of several early-induced DUSP proteins were reported between 20 and 45 min (DUSP1,4,5,6). To take this information into account, we chose rather tight upper and lower bound for the half-lives of DUSP mRNA and protein. All other parameters feature relatively loose bounds (see Table below).

	Kd_ES (nM) **	dusp_basal (nM)	dusp_ind (unitless)	Kdusp (nM)	Tdusp (min) *	v2 (nM)	TDUSP (min) *	cDUSP (nM)	STYX contr. (nM)	STYX k.d. (nM)
Lower and upper bounds	6 – 600	0.3 – 30	0 – 100	30 – 3,000	7 – 60	5 – 100	15 – 60	10 – 10,000	10 – 10,000	10 – 10,000
Best fit	263	0.908	99.7	420	20.4	14.8	21.9	11.1	8,195	1,670

Table S5. Estimated parameter values.
*The tight upper and lower bounds of the DUSP half-lives are based on kinetic information in the literature.
**Here Kd_ES denotes the ERK-STYX dissociation constant defined by Kd_ES = k2_ES/k1_ES.

Model implementation, simulation and training

The models were implemented using the Potter's Wheel toolbox for Matlab (13), which was also used for simulations and parameter estimation. We used the ppERK STYX knockdown data as a training data set for parameter estimation. To validate the model predictions, we used different validation data sets (such as the STYX overexpression data). For estimating the parameters Potter's Wheel minimises the weighted sum-of-squares differences between simulation and data (called the Chi-square function), in which the weights are given by the standard deviations of the data in each time-point (see the Potter's Wheel documentation for details). We assumed that the ppERK level in starved conditions is negligible (ppERK = 0 for $t < 0$). To account for the fact that the data obtained by Western blotting are arbitrarily scaled we also fitted a scaling parameter, i.e. the simulated data equals the model's ppERK levels multiplied by the scaling factor (this procedure is standard protocol in parameter estimation, see Hengl et al. (14) and Maiwald et al. (13) for details). To analyse identifiability and accuracy of the predictions, the estimation algorithm was run multiple times independently in order to obtain a set of good-fitting estimates (see Table in Dataset S1). This set of estimates was then analysed for parameter correlations and variability of the simulated predictions (see Fig. 4 and Fig. S3B).

In vitro phosphatase assay

The in vitro phosphatase assay was performed as described by Nyonya et al. (15) with the following changes: cells expressing either HA-pCMV, HA-STYX, HA-STYX-GC or myc-DUSP4 were lysed and the proteins were immunoprecipitated in MAPK-IP buffer (described in the main methods section) supplemented with proteinase inhibitor, but without phosphatase inhibitor using HA-agarose beads (Sigma-Aldrich) or anti-c-myc agarose beads (Sigma-Aldrich). The immunoprecipitate was washed two times in MAPK IP buffer and once in phospahatase buffer (50mM Tris-HCl PH 7.5, 1mM MgCl2, 0.1mM EDTA and 0.9mg/ml BSA). Beads were subsequently incubated with 150 ng of

recombinant GST-tagged ppERK2 (Sigma-Aldrich) in 20ul phosphatase buffer. The mixture was incubated for 20 minutes at 37°C and the reaction was terminated by boiling in sample buffer.

GST-pulldown

The GST pulldown was performed based on Zhou et al. (16). Briefly, 0.3 μg purified GST-tagged ppERK2 (Sigma-Aldrich) or GST only was bound to Glatutahion Sepharose 4 Fast Flow (GE Healthcare) in binding buffer (PBS supplemented with 1mM DTT and proteinase inhibitor) at 4°C. After binding, sepharose was washed and blocked in blocking buffer (5% BSA in PBS, 1mM DTT and proteinase inhibitor) at 4°C for 1 h. Subsequently, 0.6 μg His-tagged purified STYX (Abcam) was added in 200ul binding buffer overnight at 4°C. Sepharose was washed twice with washing buffer (binding buffer with 0.5% NP40) and once with PBS. Proteins were eluted by boiling in sample buffer.

Cloning of ERK2-TYAF

The nonphosphoryable ERK2 mutant was created using site directed mutagenesis, substituting threonine 183 by alanine and tyrosine 185 by phenylalanine.

References

1. Burack W-R. Sturgill T-W (1997) The activating dual phosphorylation of MAPK by MEK is nonprocessive. *Biochemistry* 36(20): 5929-5933.
2. Ferrell J-E., Jr., Bhatt R-R (1997) Mechanistic studies of the dual phosphorylation of mitogen-activated protein kinase. *J Biol Chem* 272(30): 19008-19016.
3. Zhao Y, Zhang Z-Y (2001) The mechanism of dephosphorylation of extracellular signal-regulated kinase 2 by mitogen-activated protein kinase phosphatase 3. *J Biol Chem* 276(34): 32382-32391.
4. Fujioka A, et al. (2006) Dynamics of the Ras/ERK MAPK cascade as monitored by fluorescent probes. *J Biol Chem* 281(13): 8917-8926.
5. Legewie S, et al. (2008) Recurrent design patterns in the feedback regulation of the mammalian signalling network. *Mol Syst Biol* 4: 190.

6. Kucharska A, Rushworth L-K, Staples C, Morrice N-A, Keyse S-M (2009) Regulation of the inducible nuclear dual-specificity phosphatase DUSP5 by ERK MAPK. *Cell Signal* 21(12): 1794-1805.
7. Nakakuki T, et al. (2010) Ligand-specific c-Fos expression emerges from the spatiotemporal control of ErbB network dynamics. *Cell* 141(5): 884-896.
8. Cagnol S, Rivard N (2012) Oncogenic KRAS and BRAF activation of the MEK/ERK signaling pathway promotes expression of dual-specificity phosphatase 4 (DUSP4/MKP2) resulting in nuclear ERK1/2 inhibition. *Oncogene [Epub ahead of print]*.
9. Kolch W (2000) Meaningful relationships: the regulation of the Ras/Raf/MEK/ERK pathway by protein interactions. *Biochem J* 351(2): 289-305.
10. Harrington H-A, Komorowski M, Beguerisse-Díaz M, Ratto G-M, Stumpf M-P (2012) Mathematical modeling reveals the functional implications of the different nuclear shuttling rates of Erk1 and Erk2. *Phys Biol* 9(3): 036001.
11. Markevich, N-I, et al. (2004) Signaling switches and bistability arising from multisite phosphorylation in protein kinase cascades. *J Cell Biol* 164(3): 353-359.
12. Fey D, Croucher D-R, Kolch W, Kholodenko B-N (2012) Crosstalk and signaling switches in mitogen-activated protein kinase cascades *Front Physiol* 3: 355.
13. Maiwald T, Timmer J (2008) Dynamical modeling and multi-experiment fitting with PottersWheel. *Bioinformatics* 24(18): 2037-2043.
14. Hengl S, Kreutz, C, Timmer J, Maiwald T (2007) Data-based identifiability analysis of non-linear dynamical models. *Bioinformatics* 23(19): 2612-2618.
15. Nyunoya T, Monick M-M, Powers L-S, Yarovinsky T-O,Hunninghake G-W (2005) Macrophages Survive Hyperoxia via Prolonged ERK Activation Due to Phosphatase Down-regulation. *J Biol Chem* 280(28):26295-26302.
16. Zhou B *et al.* (2001) Multiple Regions of MAP Kinase Phosphatase 3 Are Involved in Its Recognition and Activation by ERK2. *J Biol Chem* 276(9):6506-6515.

Supplementary figure legends

Figure S1. *A&B,* HeLa cells were serum starved for 1 h followed by stimulation with 10% FCS for the indicated time points. Cells were lysed and immunoblotted against DUSP4 (A) or STYX (B). Tubulin was detected as a loading control. STYX in panel B indicates a cell lysate from HeLa cells

overexpressing a non-tagged version of STYX. The lysate was loaded to verify the identity of the STYX band.

Figure S2. STYX does not dephosphorylate ppERK2, while DUSP4 does. HeLa cells were transfected with plasmids encoding HA-tagged STYX or myc-tagged DUSP4. After 24 h, cells were lysed and STYX was immunoprecipitated against HA and DUSP4 was immunoprecipitated against myc. The immunoprecipitate was co-incubated with purified ppERK2 for 30 min followed by SDS-PAGE and immunoblotting against the indicated proteins.

Figure S3. *A,* Detailed reaction kinetic scheme of the model. Black/grey: the common core biochemical interactions that do not involve STYX (black-grey colour scheme helps visualize the biochemical fluxes). Blue: Possible interactions with STYX considered in the different hypothetical models 1-5 as explained in the main text. *B,* Visualization of the most correlated parameter estimates. Dots indicate the individual estimates from n>30 estimation runs with the colour indicating the corresponding goodness of fit, where Chi^2/n < 1 is acceptable. STYX_C1 and STYC_C2 denote the estimated STYX concentrations in control and STYX depleted conditions, respectively and scale_cellppERK is the estimated scaling factor relating the simulated ppERK values (number of molecules) to the Western Blot data (arbitrary units).

Figure S4. The effect of STYX is not confined to a single stimulus of cell line. *A,* HeLa cells were transfected with non-targeting siRNA (control) or with siRNA against STYX (siSTYX). After 72 h, cells were serum-starved followed by stimulation with EGF (10 ng/ml) for the indicated time points. Cells were lysed and immunoblotted against the indicated proteins. *B,* HeLa cells were transfected with non-targeting siRNA (control) or with siRNA against STYX (siSTYX). After 72 h, cells were serum-starved followed by stimulation with 10% FCS (FCS) or phorbol ester (PMA, 50 ng/ml) for the indicated time points. Cells were lysed and immunoblotted against the indicated proteins. *C,* HepG2 cells were transfected with non-targeting siRNA (control) or with siRNA against STYX (siSTYX). After 72 h, cells were serum-starved followed by stimulation with 10% FCS for the indicated time points. Cells were lysed and immunoblotted against the indicated proteins. *D,* HEK293 cells were transfected with non-targeting siRNA (control) or with siRNA against STYX (siSTYX). After 72 h, cells were serum-starved followed by stimulation with 10% FCS for the indicated time points. Cells were lysed and immunoblotted against the indicated proteins.

Figure S5. The effect of STYX is not confined to a single ERK isoform. *A,* HeLa cells were transfected with non-targeting siRNA (co) or with siRNA against STYX (si). After 48 h, cells were transfected with plasmids encoding HA-tagged ERK1 or flag-tagged ERK2. After 24h, cells were serum-starved and harvested either directly (0) or followed by stimulation with 10% FCS for 0 or 10 min (10). Cell lysates were immunoblotted against ppERK (upper blot) and against HA or flag (lower blot) as a loading control. Arrows indicate the position of the position of the overexpressed ERK construct. *B,* same experiment as in panel A, except that ppERK was normalized to general ERK.

Figure S6. Purified STYX binds to purified ERK2. Purified, recombinant His-tagged STYX was co-incubated with GST or with GST-ERK2 and the material was pulled down using GSH-sepharose beads. After washing the beads, the material was eluted by boiling in sample buffer, and the eluate was subjected to SDS-PAGE followed by immunoblotting against the indicated proteins.

Figure S7. Mobility of the STYX-ERK complex. HeLa cells were transfected with plasmids encoding YFP1-tagged ERK2 and YFP2-tagged STYX. After 24 h, FRAP experiment was performed by bleaching the cytosolic area. Images displayed are those acquired before bleaching (pre-bleach), directly after bleaching the cytosol (post-bleach) and at the end of the 60 sec recovery phase (recovery). Note that the cytosol barely recovers after photobleaching.

Figure S8. STYX and DUSP4 compete for binding to ERK independently of ERK catalytic activity and phosphorylation. *A,* HeLa cells in 10 cm cell culture dishes were transfected with plasmids encoding flag-ERK2 (wild type) and YFP-STYX together with either empty vector (-), or with 3 μg DUSP4 (low), or with 5.4 μg DUSP4 (high). After 24 h, cells were serum-starved for 2 h followed by stimulation with 10% FCS. Cells were lysed and the lysates were subjected to immunoprecipitation against flag (ERK2) and immunoblotted against indicated proteins. 3% of the lysate was used as an input control. *B,* HeLa cells in 10 cm cell culture dishes were transfected with plasmids encoding flag-ERK2-K52R (catalytically dead) and YFP-STYX together with either empty vector (-), or with 3 μg DUSP4 (low), or with 5.4 μg DUSP4 (high). After 24 h, cells were serum-starved for 2 h followed by stimulation with 10% FCS. Cells were lysed and the lysates were subjected to immunoprecipitation against flag (ERK2) and immunoblotted against indicated proteins. 3% of the lysate was used as an input control. *C,* HeLa cells in 10 cm cell culture dishes were transfected with plasmids encoding flag-ERK2-TYAF (non-phosphorylatable) and YFP-STYX together with either empty vector (-), or with 3 μg DUSP4 (low), or with 5.4 μg DUSP4 (high). After 24 h, cells were serum-starved for 2 h

followed by stimulation with 10% FCS. Cells were lysed and the lysates were subjected to immunoprecipitation against flag (ERK2) and immunoblotted against indicated proteins. 3% of the lysate was used as an input control.

Figure S9. ERK2-TYAF is not phosphorylatable. HeLa cells were transfected with plasmids encoding flag-tagged wild type ERK2 (ERK2-WT), catalytically dead ERK2 (ERK2-K52R) or an ERK2 mutant with mutated phosphorylation sites (ERK2-TYAF). After 24 h, cells were serum-starved and harvested (-) or stimulated with 10% FCS (+) for 10 min followed by lysis. Lysates were subjected to SDS-PAGE followed by immunoblotting against the indicated proteins. Arrow indicates the position of overexpressed ERK2 constructs and arrow heads indicate the positions of endogenous ERK1/2.

Figure S10. All ERK2 versions bind DUSP4. HeLa cells were transfected with plasmids encoding flag-tagged wild type ERK2 (WT), catalytically dead ERK2 (K52R) or a non-phosphorylatable mutant (TYAF). Cells were lysed after 24 h and the ERK2 was immunoprecipitated against flag. The immunoprecipitate was eluted followed by SDS-PAGE and immunoblotting against the indicated proteins. 3% of the lysate was used as an input control.

Figure S11. Effect of STYX overexpression on GATA transcriptional activity. HeLa cells were transfected with empty vector or with a plasmid encoding HA-tagged STYX (HA-STYX) together with GATA-luciferase reporter and a renilla luciferase vector. After 8 h, cells were serum-starved for 16 h and luciferase activity was assessed using the Dual-Luciferase Reporter Assay System ® (Promega) according to manufacturer's instructions.

#	Reaction	Forward rate	Reverse rate	Parameter values	Model version*				
					1	2	3	4	5
i) ERK phosphorylation									
1	ERKc + MEK* ⇌ ERK-M*	$k1_{ERKc}$ ERKc MEK*	$k2_{ERKc}$ ERK-M*	$k1_{ERKc} = 1\ min^{-1}\ nM^{-1}$ $k2_{ERKc} = 350\ min^{-1}$	x	x	x	x	x
2	ERK-M* ⇀ pERKc + MEK*	$k3_{ERKc}$ ERK-M*	–	$k3_{ERKc} = 13.2\ min^{-1}$	x	x	x	x	x
3	pERKc + MEK* ⇌ pERK-M*	$k1_{pERKc}$ pERKc MEK*	$k2_{pERKc}$ pERK-M*	$k1_{pERKc} = 1\ min^{-1}\ nM^{-1}$ $k2_{pERKc} = 350\ min^{-1}$	x	x	x	x	x
4	pERK-M* ⇀ ppERKc + MEK*	$k3_{pERKc}$ pERK-M*	–	$k3_{pERKc} = 13.2\ min^{-1}$	x	x	x	x	x
ii) ERK nuclear shuttling				Vc = 0.94 pl, Vn = 0.22 pl					
5a	ERKc ⇌ ERKn	k_{ERKin} ERKc Vc	k_{ERKout} ERKn Vn (for models 1-4)	$k_{ERKin} = 0.144\ min^{-1}$ $k_{ERKout} = 1.08\ min^{-1}$	x	x	x	x	-
5b	ERKc ⇌ ERKn	k_{ERKin} ERKc Vc	k_{ERKout} STYX ERKn Vn (for model 5)	$k_{ERKin} = 0.144\ min^{-1}$ $k_{ERKout} = 2.16e\text{-}4\ min^{-1}\ nM^{-1}$	-	-	-	-	x
6	pERKc ⇌ pERKn	k_{pERKin} pERKc Vc	$k_{pERKout}$ pERKn Vn	$k_{pERKin} = 0.144\ min^{-1}$ $k_{pERKout} = 1.08\ min^{-1}$	x	x	x	x	x
7a	ppERKc ⇌ ppERKn	$k_{ppERKin}$ ppERKc Vc (for models 1-3, 5)	$k_{ppERKout}$ ppERKn Vn	$k_{ppERKin} = 0.66\ min^{-1}$ $k_{ppERKout} = 0.78\ min^{-1}$	x	x	x	-	x
7b	ppERKc ⇌ ppERKn	$k_{ppERKin}$ ppERKc STYX Vc (for model 4)	$k_{ppERKout}$ ppERKn Vn	$k_{ppERKin} = 1.32e\text{-}4\ min^{-1}\ nM^{-1}$ $k_{ppERKout} = 0.78\ min^{-1}$	-	-	-	x	-
iii) ERK dephosphorylation									
8	ppERKc + cDUSP ⇌ ppE-cD	$kd1_{ppERKc}$ ppERKc cDUSP	$kd2_{ppERKc}$ ppE-cD	$kd1_{ppERKc} = 1\ min^{-1}\ nM^{-1}$ $kd2_{ppERKc} = 60\ min^{-1}$	x	x	x	x	x
9	ppE-cD* ⇀ pERKc + cDUSP	$kd3_{ppERKc}$ ppE-cD	–	$kd3_{ppERKc} = 0.388\ min^{-1}$	x	x	x	x	x
10	pERKc + cDUSP ⇌ pE-cD	$kd1_{pERKc}$ pERKc cDUSP	$kd2_{pERKc}$ pE-cD	$kd1_{pERKc} = 1\ min^{-1}\ nM^{-1}$ $kd2_{pERKc} = 160\ min^{-1}$	x	x	x	x	x
11	pE-cD* ⇀ ERKc + cDUSP	$kd3_{pERKc}$ pE-cD	–	$kd3_{pERKc} = 0.432\ min^{-1}$	x	x	x	x	x
12	ppERKn + nDUSP ⇌ ppE-nD	$kd1_{ppERKn}$ ppERKn nDUSP	$kd2_{ppERKn}$ ppE-nD	$kd1_{ppERKn} = 1\ min^{-1}\ nM^{-1}$ $kd2_{ppERKn} = 60\ min^{-1}$	x	x	x	x	x
13	ppE-nD* ⇀ pERKn + nDUSP	$kd3_{ppERKn}$ ppE-nD	–	$kd3_{ppERKn} = 38.8\ min^{-1}$	x	x	x	x	x

14	$pERKn + nDUSP \rightleftharpoons pE\text{-}nD$	$kd1_{pERKn}$ pERKn nDUSP	$kd2_{pERKn}$ pE-nD	$kd1_{pERKn} = 1\ min^{-1}\ nM^{-1}$ $kd2_{pERKn} = 160\ min^{-1}$	x	x	x	x	x
15	$pE\text{-}nD^* \rightharpoonup ERKn + nDUSP$	$kd3_{pERKn}$ pE-nD	—	$kd3_{pERKn} = 43.2\ min^{-1}$	x	x	x	x	x
iv) DUSP expression									
16	$\emptyset \xrightarrow{ppERKn} dusp$	$dusp_{basal}\left(1 + dusp_{ind}\frac{ppERKn^2}{K_{dusp} + ppERKn^2}\right)\frac{\log(2)}{Tdusp}$	—	$dusp_{basal} = 1\ nM$ $dusp_{ind} = 20$ $K_{dusp} = 1000\ nM$	x	x	x	x	x
17	$dusp \rightharpoonup \emptyset$	$dusp\ \log(2)/T_{dusp}$	—	$T_{dusp} = 10\ min$	x	x	x	x	x
18	$\emptyset \xrightarrow{dusp} DUSPn$	$v2\ dusp\ \log(2)/T_{DUSP}$	—	$v2 = 10$	x	x	x	x	x
19	$DUSPn \rightharpoonup \emptyset$	$DUSPn\ \log(2)/T_{DUSP}$	—	$T_{DUSP} = 45\ min$	x	x	x	x	x
v) STYX-ERK binding									
20	$ERKn + STYX \rightleftharpoons E\text{-}S$	$k1_{ES}$ ERKn STYXn	$k2_{ES}$ E-S	$k1_{ES} = 1\ min^{-1}\ nM^{-1}$ $k2_{ES} = 160\ min^{-1}$	x	x	-	-	-
21	$pERKn + STYX \rightleftharpoons pE\text{-}S$	$k1_{ES}$ pERKn STYXn	$k2_{ES}$ pE-S	$k1_{ES} = 1\ min^{-1}\ nM^{-1}$ $k2_{ES} = 160\ min^{-1}$	x	-	-	-	-
22	$ppERKn + STYX \rightleftharpoons ppE\text{-}S$	$k1_{ES}$ ppERKn STYXn	$k2_{ES}$ ppE-S	$k1_{ES} = 1\ min^{-1}\ nM^{-1}$ $k2_{ES} = 160\ min^{-1}$	x	-	x	-	-

* An x-mark "x" indicates that this reaction is present in the model corresponding to this column, a dash "-" indicates that this reaction is absent.

Model 1

#	Differential equation	Compartment	Initial condition
1	$d/dt\ ERKc = -v1 - v5a/Vc + v11$	Cytosol	572.5 nM
2	$d/dt\ pERKc = v2 - v3 - v6/Vc + v9 - v10$	″	0
3	$d/dt\ ppERKc = v4 - v7a/Vc - v8$	″	0
4	$d/dt\ ERK\text{-}ppMEKc = v1 - v2$	″	0
5	$d/dt\ pERK\text{-}ppMEKc = v3 - v4$	″	0
6	$d/dt\ DUSPc = -v8 + v9 - v10 + v11$	″	100 nM
7	$d/dt\ pERK\text{-}DUSPc = v10 - v11$	″	0
8	$d/dt\ ppERK\text{-}DUSPc = v8 - v9$	″	0
9	$d/dt\ ERKn = v5a/Vn + v15 - v20$	Nucleus	1630.9 nM
10	$d/dt\ pERKn = v6/Vn + v13 - v14 - v21$	″	0
11	$d/dt\ ppERKn = v7a/Vn - v12 - v22$	″	0
12	$d/dt\ pERK\text{-}DUSPn = v14 - v15$	″	0
13	$d/dt\ ppERK\text{-}DUSPn = v12 - v13$	″	0
14	$d/dt\ STYXn = -v20 - v21 - v22$	″	5000 nM (for control) 500 nM (for k.d.)
15	$d/dt\ ERK\text{-}STYXn = v20$	″	0
16	$d/dt\ pERK\text{-}STYXn = v21$	″	0
17	$d/dt\ ppERK\text{-}STYXn = v22$	″	0
18	$d/dt\ duspn = v16 - v17$	″	1 nM
19	$d/dt\ DUSPn = -v12 + v13 - v14 + v15 + v18 - v19$	″	10 nM
	Algebraic equation: $MEK^* = u(t) - ERK\text{-}M^* - pERK\text{-}M^*$	Cytosol	$u(t) = 0$ nM for $t<0$ $u(t) = 100$ nM for $t\geq 0$

Model 2

#	Differential equation	Compartment	Initial condition
1	$d/dt\ ERKc = -v1 - v5a/Vc + v11$	Cytosol	572.5 nM
2	$d/dt\ pERKc = v2 - v3 - v6/Vc + v9 - v10$	″	0
3	$d/dt\ ppERKc = v4 - v7a/Vc - v8$	″	0
4	$d/dt\ ERK\text{-}ppMEKc = v1 - v2$	″	0
5	$d/dt\ pERK\text{-}ppMEKc = v3 - v4$	″	0
6	$d/dt\ DUSPc = -v8 + v9 - v10 + v11$	″	100 nM
7	$d/dt\ pERK\text{-}DUSPc = v10 - v11$	″	0
8	$d/dt\ ppERK\text{-}DUSPc = v8 - v9$	″	0
9	$d/dt\ ERKn = v5a/Vn + v15 - v20$	Nucleus	1630.9 nM
10	$d/dt\ pERKn = v6/Vn + v13 - v14$	″	0
11	$d/dt\ ppERKn = v7a/Vn - v12$	″	0
12	$d/dt\ pERK\text{-}DUSPn = v14 - v15$	″	0
13	$d/dt\ ppERK\text{-}DUSPn = v12 - v13$	″	0
14	$d/dt\ STYXn = -v20$	″	5000 nM (for control) 500 nM (for k.d.)
15	$d/dt\ ERK\text{-}STYXn = v20$	″	0
16	$d/dt\ pERK\text{-}STYXn = 0$	″	0
17	$d/dt\ ppERK\text{-}STYXn = 0$	″	0
18	$d/dt\ dusp = v16 - v17$	″	1 nM
19	$d/dt\ DUSPn = -v12 + v13 - v14 + v15 + v18 - v19$	″	10 nM
	Algebraic equation: $MEK^* = u(t) - ERK\text{-}M^* - pERK\text{-}M^*$	Cytosol	$u(t) = 0$ nM for $t<0$ $u(t) = 100$ nM for $t\geq 0$

Model 3

#	Differential equation	Compartment	Initial condition
1	$d/dt\ ERKc = -v1 - v5a/Vc + v11$	Cytosol	572.5 nM
2	$d/dt\ pERKc = v2 - v3 - v6/Vc + v9 - v10$	″	0
3	$d/dt\ ppERKc = v4 - v7a/Vc - v8$	″	0
4	$d/dt\ ERK\text{-}ppMEKc = v1 - v2$	″	0
5	$d/dt\ pERK\text{-}ppMEKc = v3 - v4$	″	0
6	$d/dt\ DUSPc = -v8 + v9 - v10 + v11$	″	100 nM
7	$d/dt\ pERK\text{-}DUSPc = v10 - v11$	″	0

8	$d/dt\ ppERK\text{-}DUSPc = v8 - v9$	″	0
9	$d/dt\ ERKn = v5a/Vn + v15$	Nucleus	1630.9 nM
10	$d/dt\ pERKn = v6/Vn + v13 - v14$	″	0
11	$d/dt\ ppERKn = v7a/Vn - v12 - v22$	″	0
12	$d/dt\ pERK\text{-}DUSPn = v14 - v15$	″	0
13	$d/dt\ ppERK\text{-}DUSPn = v12 - v13$	″	0
14	$d/dt\ STYXn = -v22$	″	5000 nM (for control) 500 nM (for k.d.)
15	$d/dt\ ERK\text{-}STYXn = 0$	″	0
16	$d/dt\ pERK\text{-}STYXn = 0$	″	0
17	$d/dt\ ppERK\text{-}STYXn = v22$	″	0
18	$d/dt\ duspn = v16 - v17$	″	1 nM
19	$d/dt\ DUSPn = -v12 + v13 - v14 + v15 + v18 - v19$	″	10 nM
	Algebraic equation: $MEK^* = u(t) - ERK\text{-}M^* - pERK\text{-}M^*$	Cytosol	$u(t) = 0$ nM for $t<0$ $u(t) = 100$ nM for $t\geq 0$

Model 4

#	Differential equation	Compartment	Initial condition
1	$d/dt\ ERKc = -v1 - v5a/Vc + v11$	Cytosol	572.5 nM
2	$d/dt\ pERKc = v2 - v3 - v6/Vc + v9 - v10$	″	0
3	$d/dt\ ppERKc = v4 - v7b/Vc - v8$	″	0
4	$d/dt\ ERK\text{-}ppMEKc = v1 - v2$	″	0
5	$d/dt\ pERK\text{-}ppMEKc = v3 - v4$	″	0
6	$d/dt\ DUSPc = -v8 + v9 - v10 + v11$	″	100 nM
7	$d/dt\ pERK\text{-}DUSPc = v10 - v11$	″	0
8	$d/dt\ ppERK\text{-}DUSPc = v8 - v9$	″	0
9	$d/dt\ ERKn = v5a/Vn + v15$	Nucleus	1630.9 nM
10	$d/dt\ pERKn = v6/Vn + v13 - v14$	″	0
11	$d/dt\ ppERKn = v7b/Vn - v12$	″	0
12	$d/dt\ pERK\text{-}DUSPn = v14 - v15$	″	0
13	$d/dt\ ppERK\text{-}DUSPn = v12 - v13$	″	0
14	$d/dt\ STYXn = 0$	″	5000 nM (for control) 1000 nM (for k.d.)
15	$d/dt\ ERK\text{-}STYXn = 0$	″	0
16	$d/dt\ pERK\text{-}STYXn = 0$	″	0
17	$d/dt\ ppERK\text{-}STYXn = 0$	″	0
18	$d/dt\ duspn = v16 - v17$	″	1 nM
19	$d/dt\ DUSPn = -v12 + v13 - v14 + v15 + v18 - v19$	″	10 nM
	Algebraic equation: $MEK^* = u(t) - ERK\text{-}M^* - pERK\text{-}M^*$	Cytosol	$u(t) = 0$ nM for $t<0$ $u(t) = 100$ nM for $t\geq 0$

Model 5

#	Differential equation	Compartment	Initial condition
1	$d/dt\ ERKc = -v1 - v5b/Vc + v11$	Cytosol	572.5 nM
2	$d/dt\ pERKc = v2 - v3 - v6/Vc + v9 - v10$	″	0
3	$d/dt\ ppERKc = v4 - v7a/Vc - v8$	″	0
4	$d/dt\ ERK\text{-}ppMEKc = v1 - v2$	″	0
5	$d/dt\ pERK\text{-}ppMEKc = v3 - v4$	″	0
6	$d/dt\ DUSPc = -v8 + v9 - v10 + v11$	″	100 nM
7	$d/dt\ pERK\text{-}DUSPc = v10 - v11$	″	0
8	$d/dt\ ppERK\text{-}DUSPc = v8 - v9$	″	0
9	$d/dt\ ERKn = v5b/Vn + v15$	Nucleus	1630.9 nM
10	$d/dt\ pERKn = v6/Vn + v13 - v14$	″	0
11	$d/dt\ ppERKn = v7a/Vn - v12$	″	0
12	$d/dt\ pERK\text{-}DUSPn = v14 - v15$	″	0
13	$d/dt\ ppERK\text{-}DUSPn = v12 - v13$	″	0
14	$d/dt\ STYXn = 0$	″	5000 nM (for control) 1000 nM (for k.d.)
15	$d/dt\ ERK\text{-}STYXn = 0$	″	0

16	$d/dt\ pERK\text{-}STYXn = 0$	″	0
17	$d/dt\ ppERK\text{-}STYXn = 0$	″	0
18	$d/dt\ duspn = v16 - v17$	″	1 nM
19	$d/dt\ DUSPn = -v12 + v13 - v14 + v15 + v18 - v19$	″	10 nM
	Algebraic equation: $MEK^* = u(t) - ERK\text{-}M^* - pERK\text{-}M^*$	Cytosol	$u(t) = 0$ nM for $t<0$ $u(t) = 100$ nM for $t\geq 0$

Figure S1

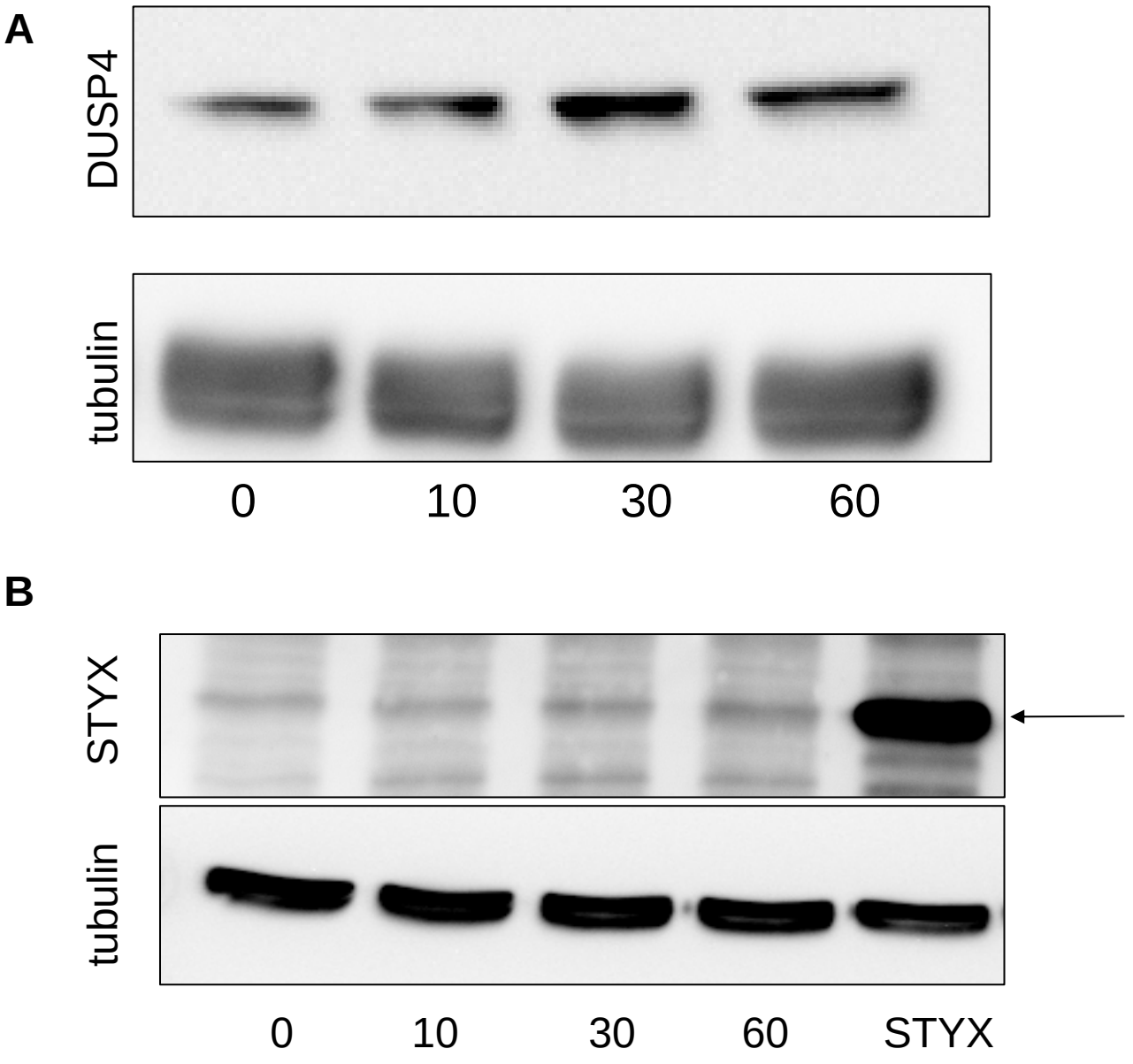

Figure S2-R

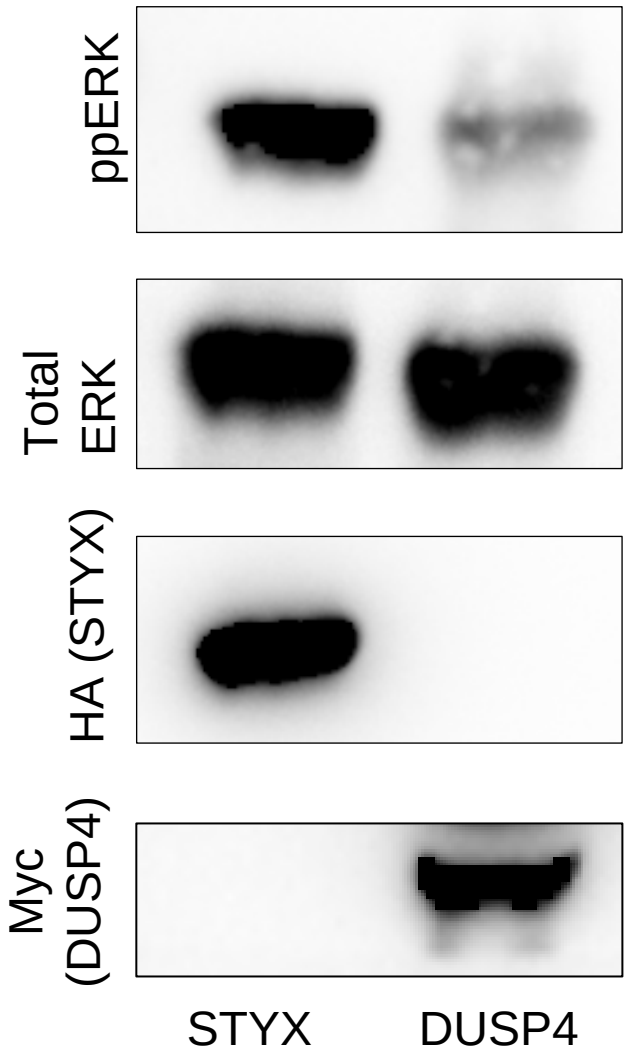

Figure S3-R

A

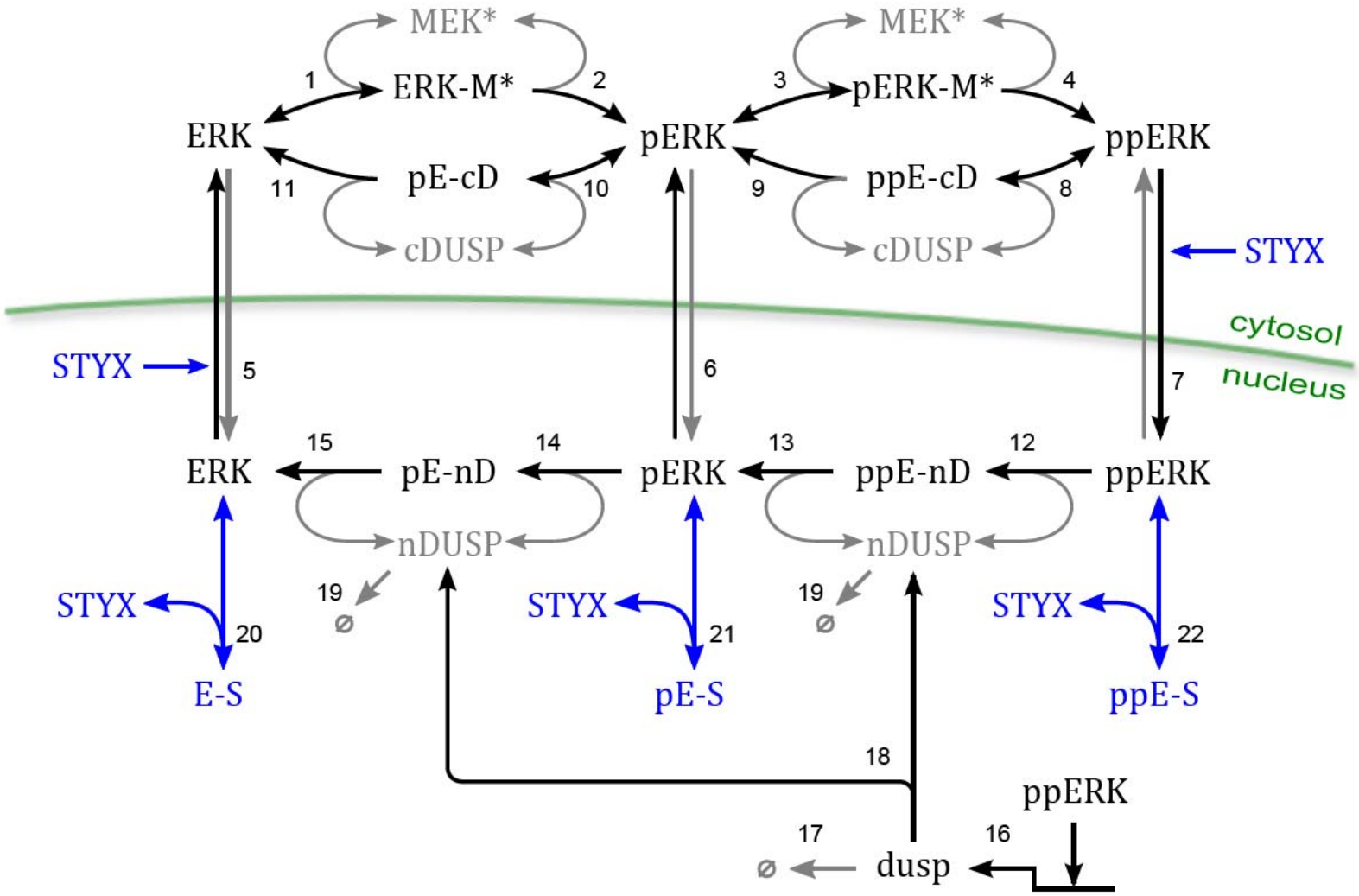
MEK*
ERK-M*
ERK
pE-cD
cDUSP
pERK
MEK*
pERK-M*
ppE-cD
cDUSP
ppERK
STYX
cytosol
nucleus
STYX
ERK
pE-nD
nDUSP
pERK
ppE-nD
nDUSP
ppERK
STYX
STYX
STYX
E-S
pE-S
ppE-S
ppERK
dusp
1
2
3
4
5
6
7
8
9
10
11
12
13
14
15
16
17
18
19
19
20
21
22

B

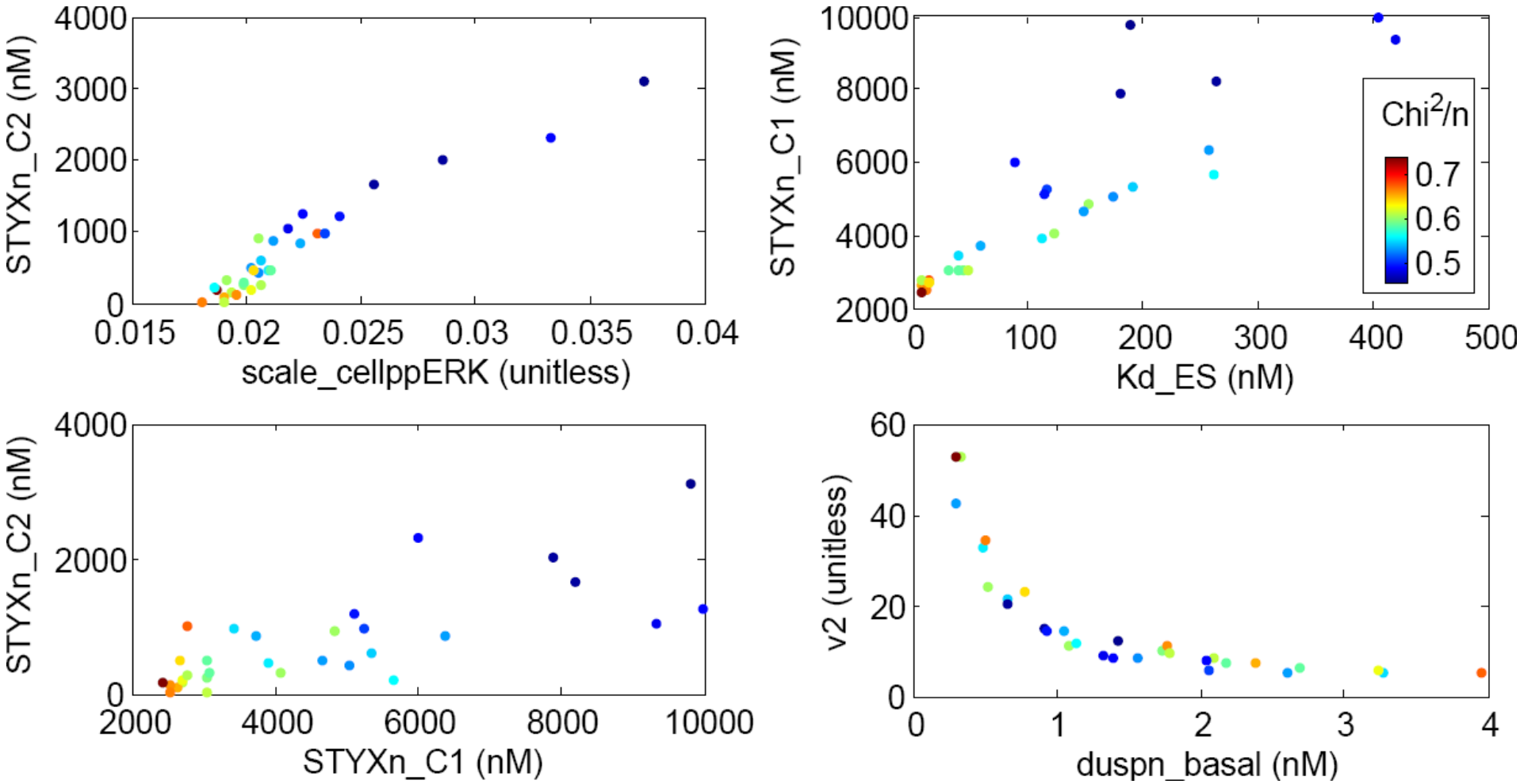
STYXn_C2 (nM)
scale_cellppERK (unitless)
STYXn_C1 (nM)
Kd_ES (nM)
Chi2/n
0.7
0.6
0.5
STYXn_C2 (nM)
STYXn_C1 (nM)
v2 (unitless)
duspn_basal (nM)

Figure S4-R

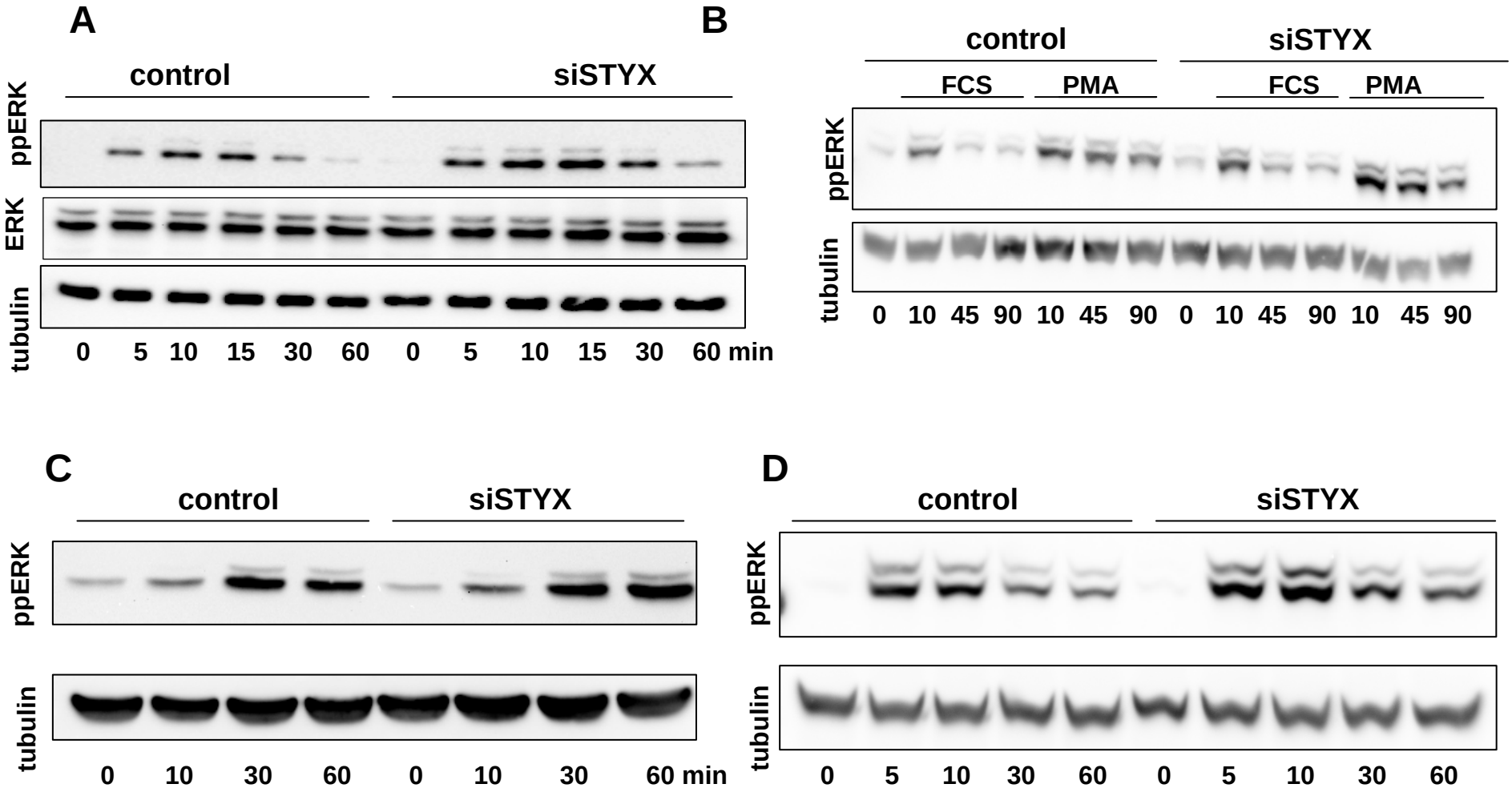
A
control
siSTYX
ppERK
ERK
tubulin
0 5 10 15 30 60 0 5 10 15 30 60 min
B
control
siSTYX
FCS
PMA
FCS
PMA
ppERK
tubulin
0 10 45 90 10 45 90 0 10 45 90 10 45 90
C
control
siSTYX
ppERK
tubulin
0 10 30 60 0 10 30 60 min
D
control
siSTYX
ppERK
tubulin
0 5 10 30 60 0 5 10 30 60

Figure S5-R

A

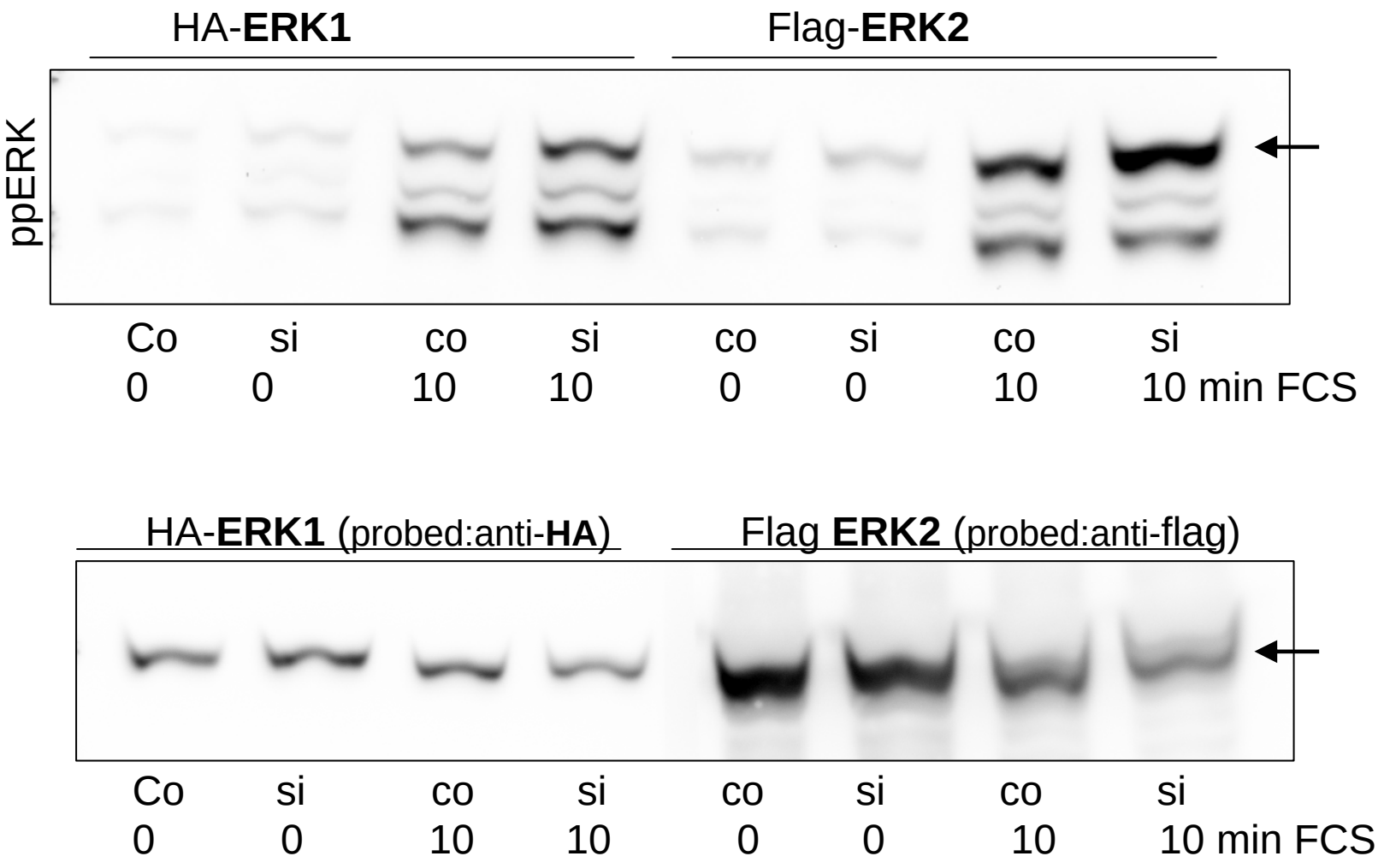
HA-**ERK1**
Flag-**ERK2**
ppERK
Co si co si co si co si
0 0 10 10 0 0 10 10 min FCS
HA-**ERK1** (probed:anti-**HA**)
Flag **ERK2** (probed:anti-flag)
Co si co si co si co si
0 0 10 10 0 0 10 10 min FCS

B

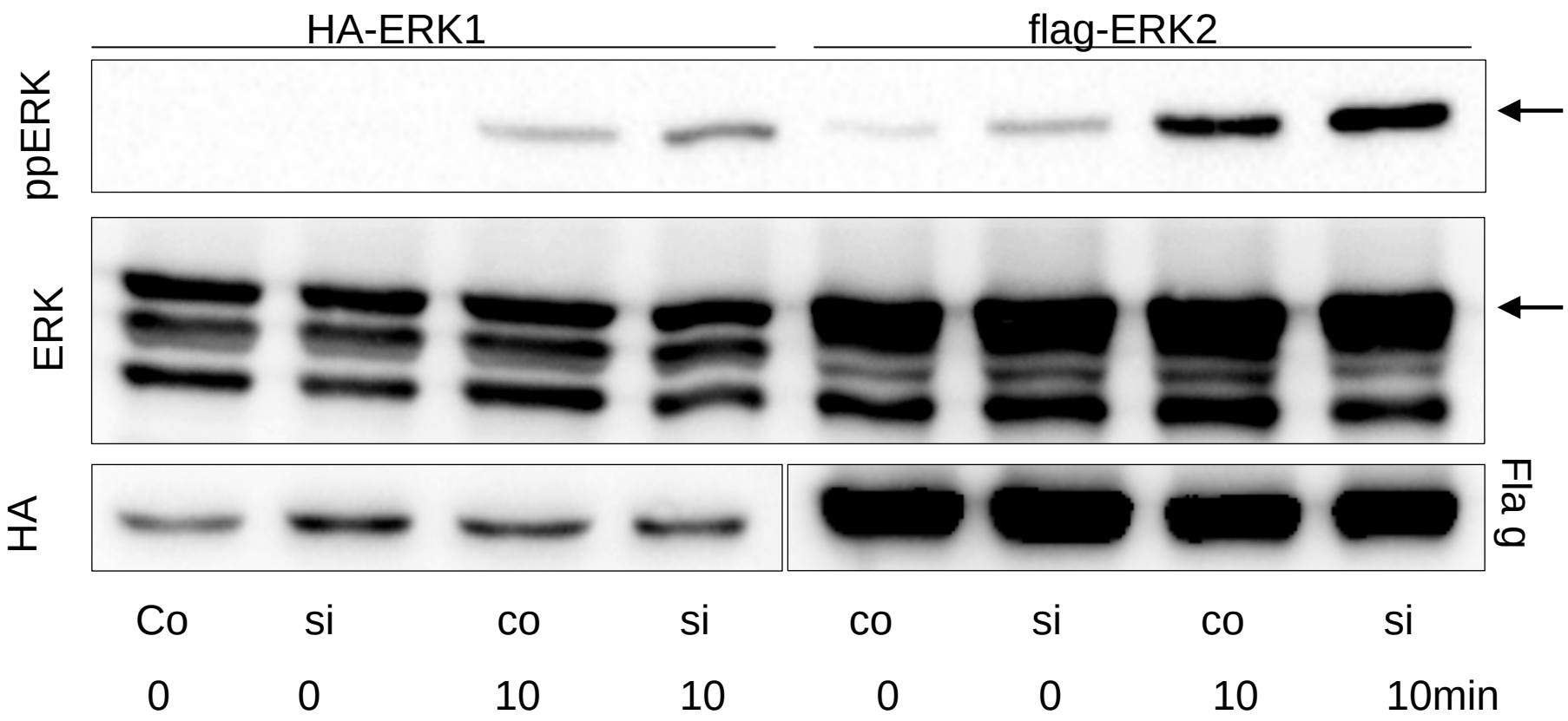
HA-ERK1
flag-ERK2
ppERK
ERK
HA
Flag
Co
si
co
si
co
si
co
si
0
0
10
10
0
0
10
10min

Figure S6-R

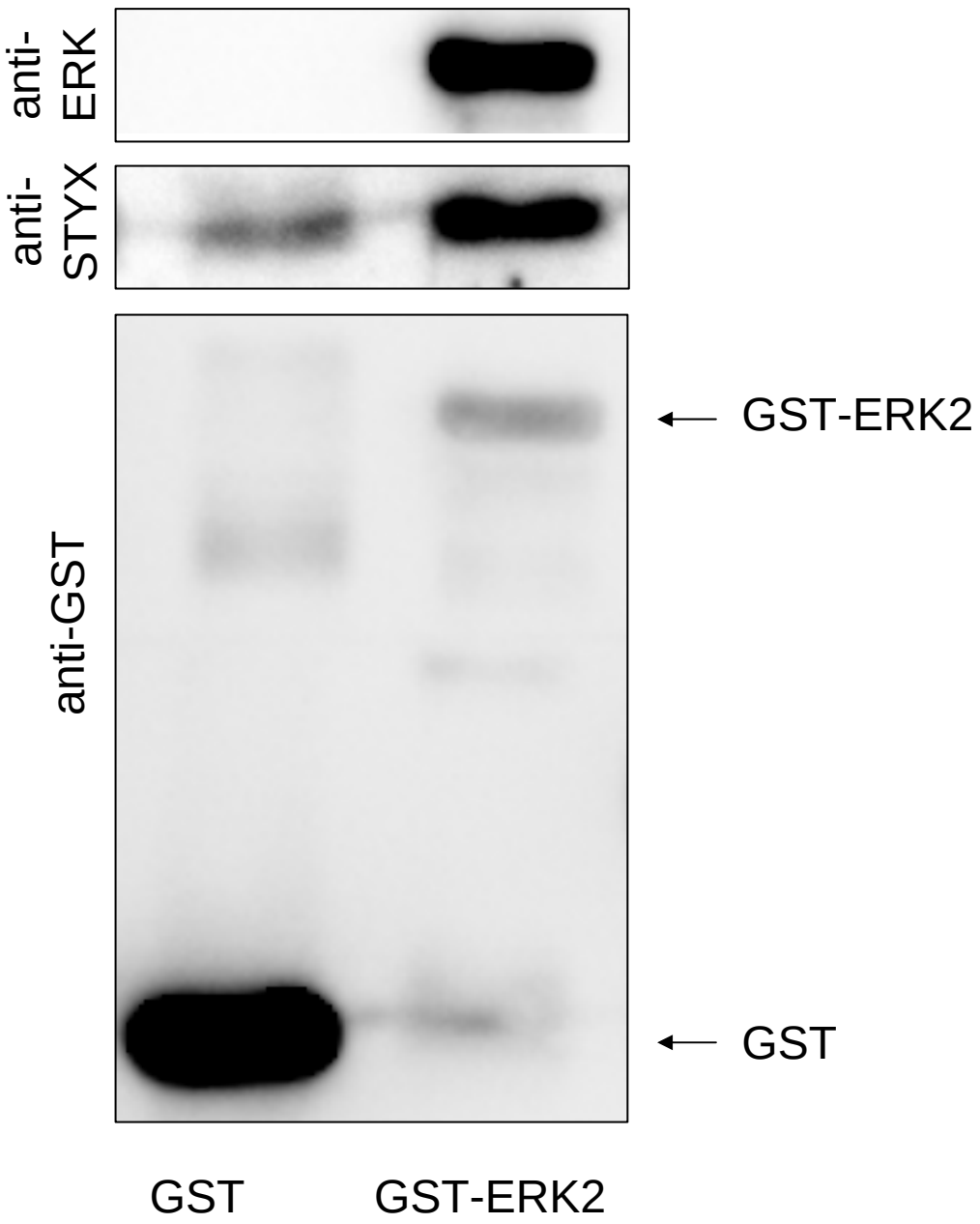

Figure S7-R

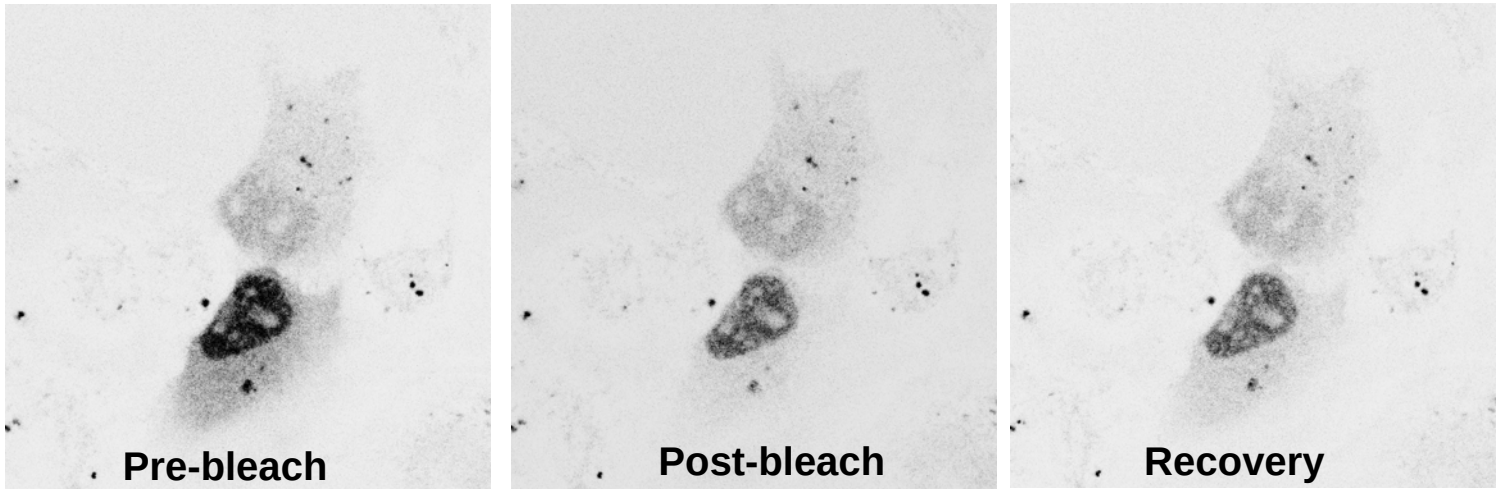

Figure S8-R

A

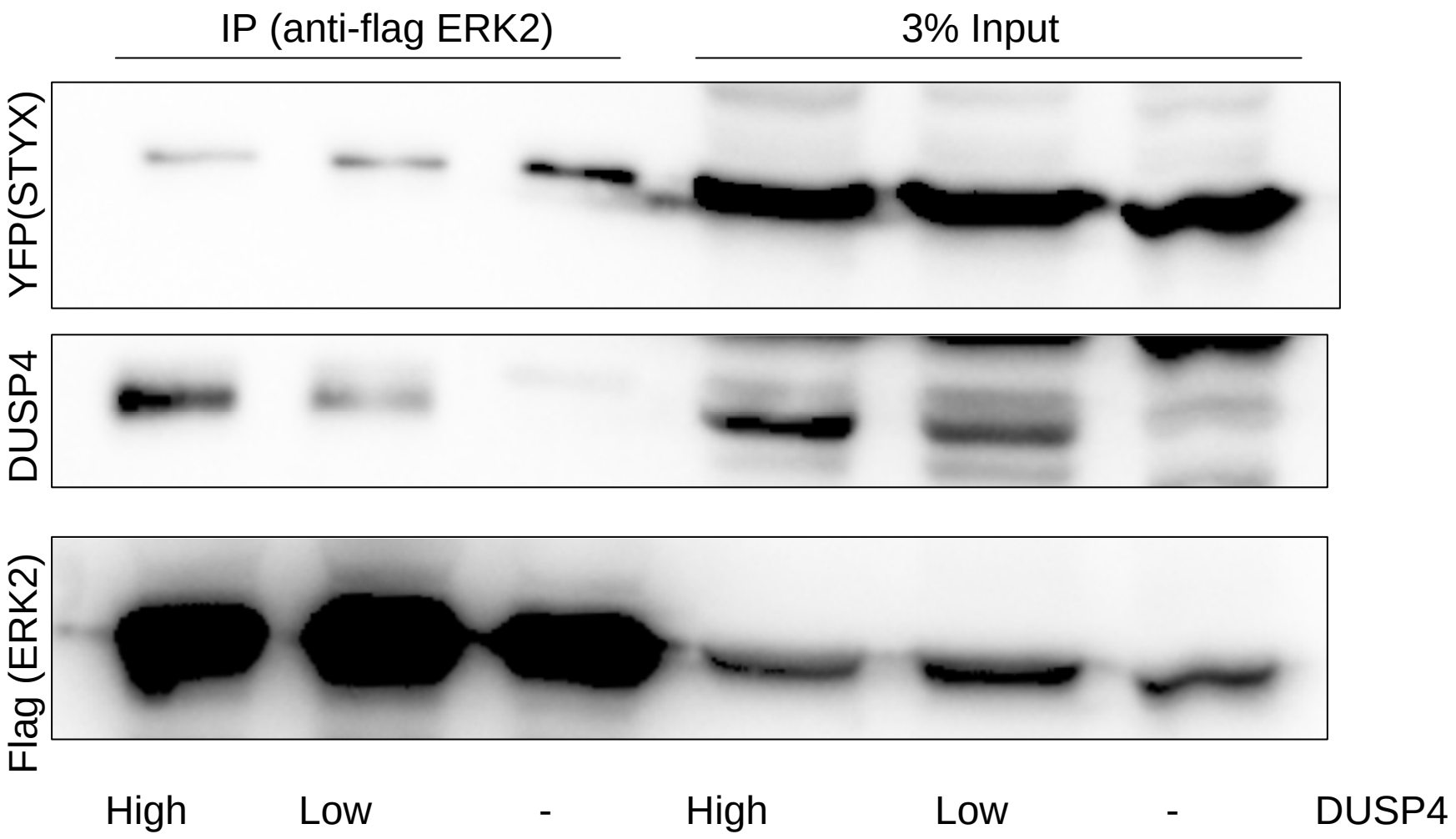
IP (anti-flag ERK2)
3% Input
YFP(STYX)
DUSP4
Flag (ERK2)
High
Low
-
High
Low
-
DUSP4

B

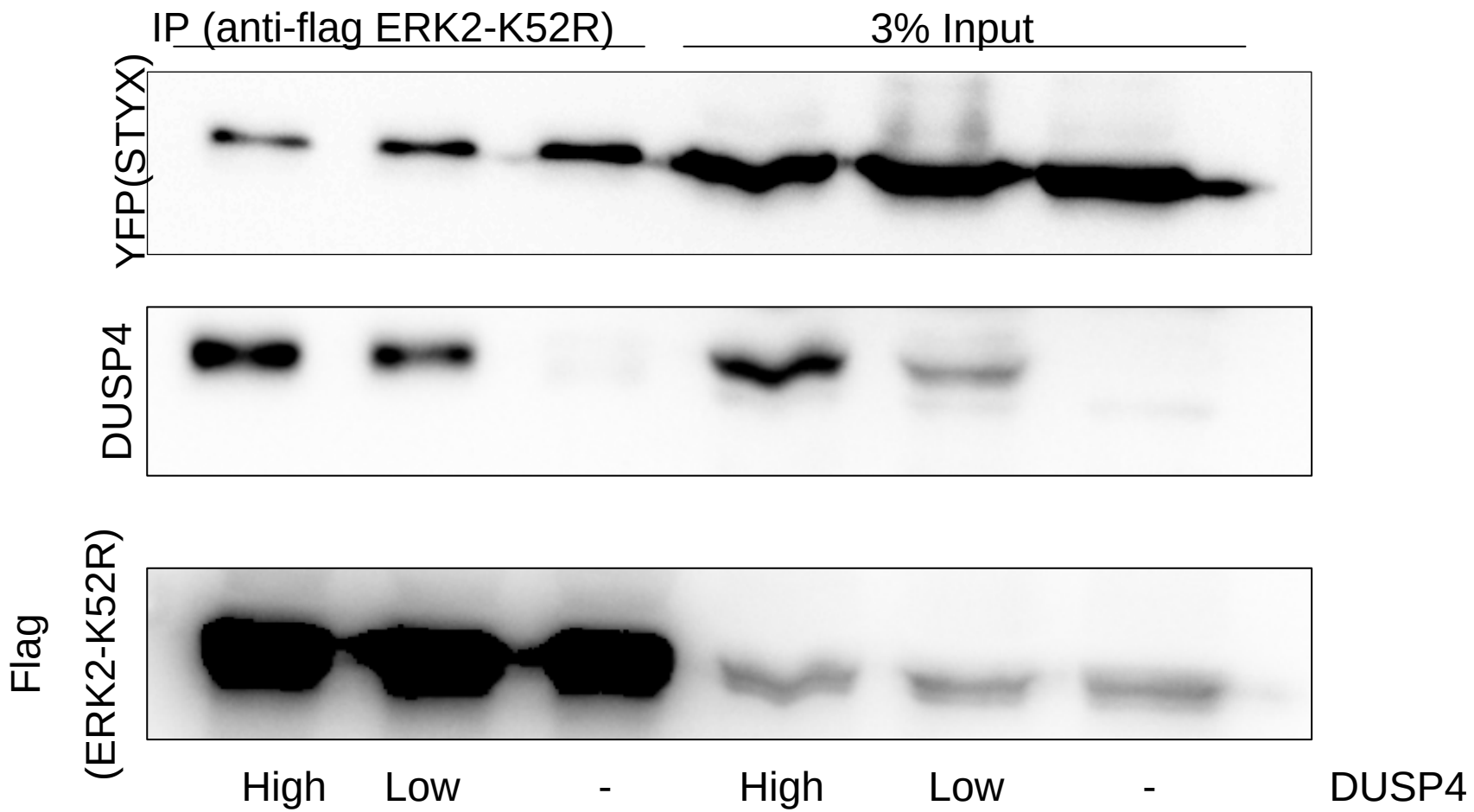
IP (anti-flag ERK2-K52R)
3% Input
YFP(STYX)
DUSP4
Flag
(ERK2-K52R)
High
Low
-
High
Low
-
DUSP4

C

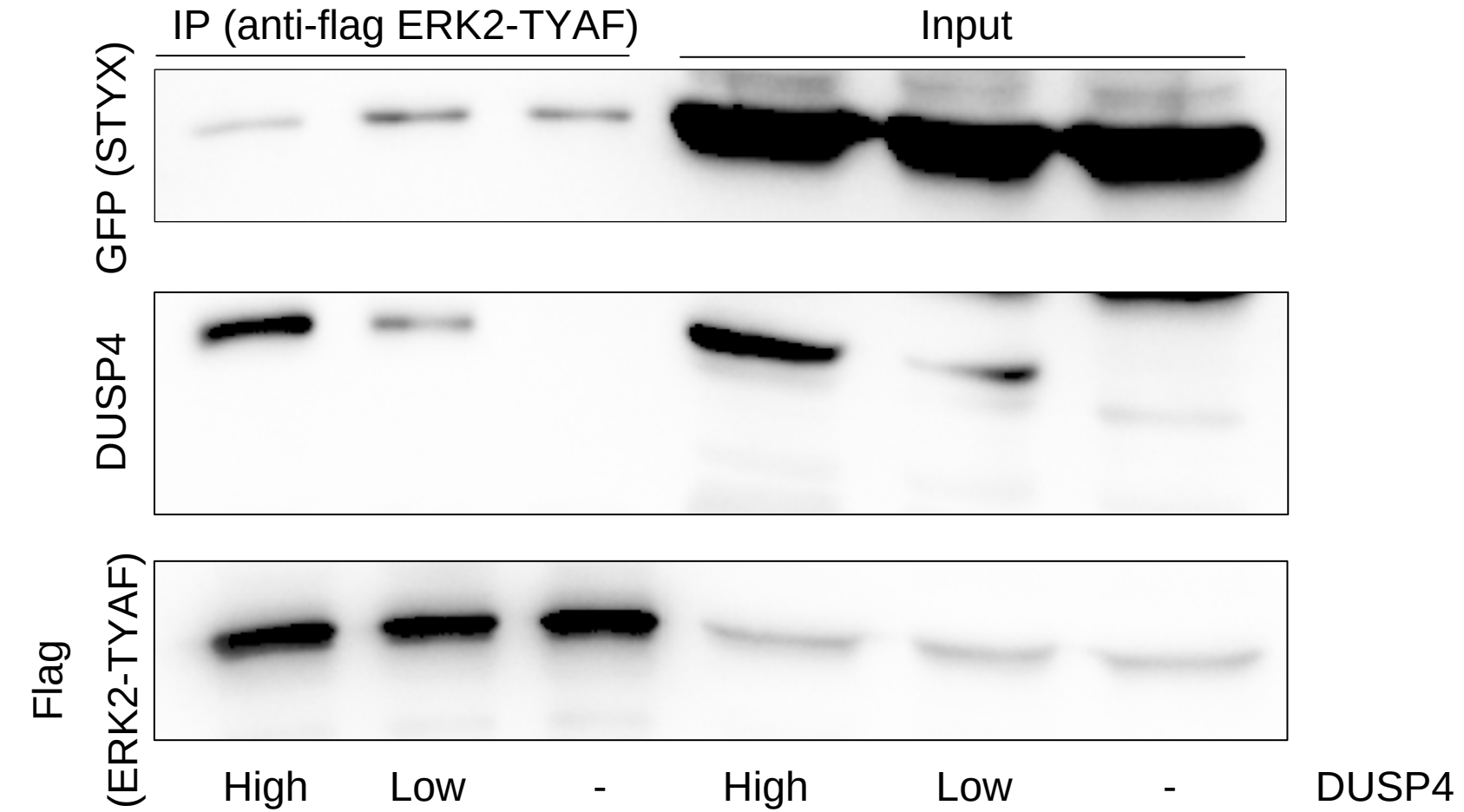
IP (anti-flag ERK2-TYAF)
Input
GFP (STYX)
DUSP4
Flag
(ERK2-TYAF)
High
Low
-
High
Low
-
DUSP4

Figure S9-R

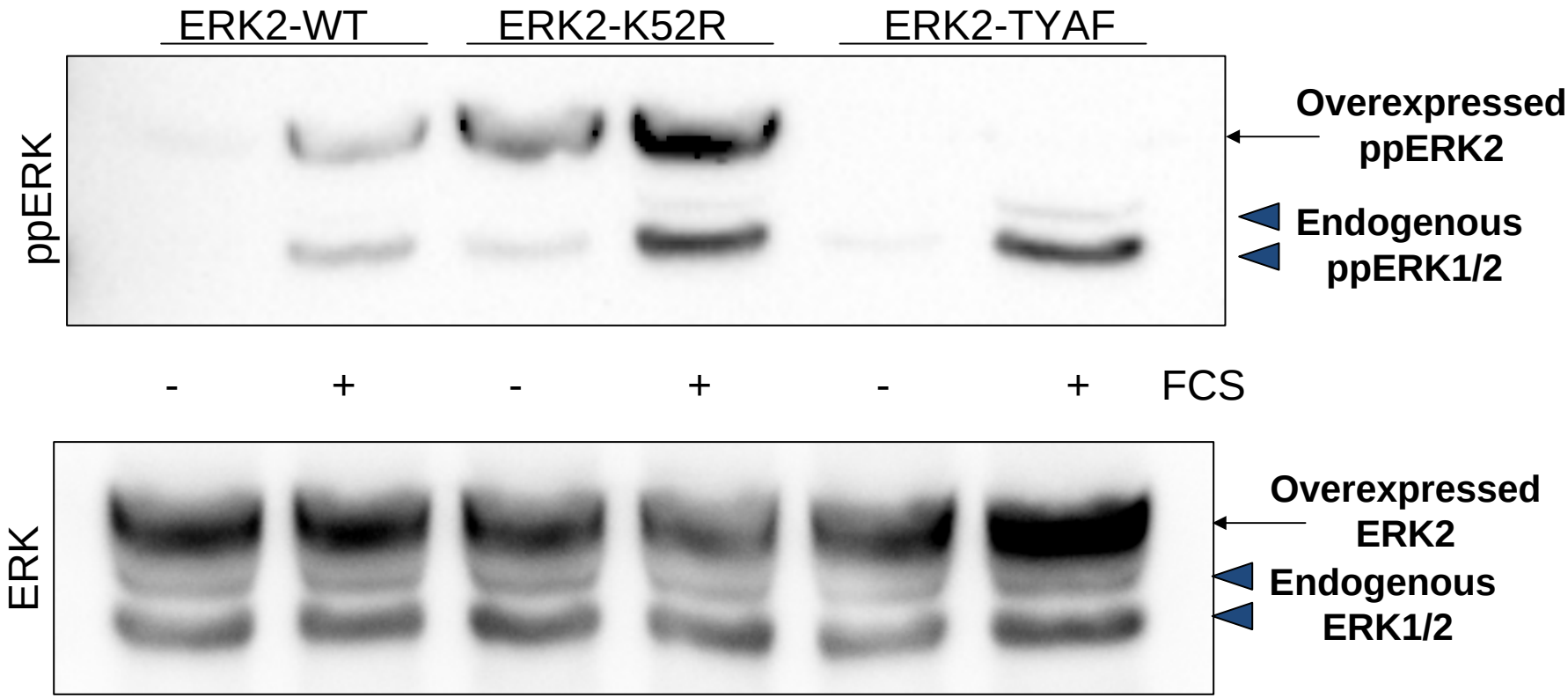
ERK2-WT
ERK2-K52R
ERK2-TYAF
ppERK
Overexpressed ppERK2
Endogenous ppERK1/2
- + - + - + FCS
ERK
Overexpressed ERK2
Endogenous ERK1/2

Figure S10-R

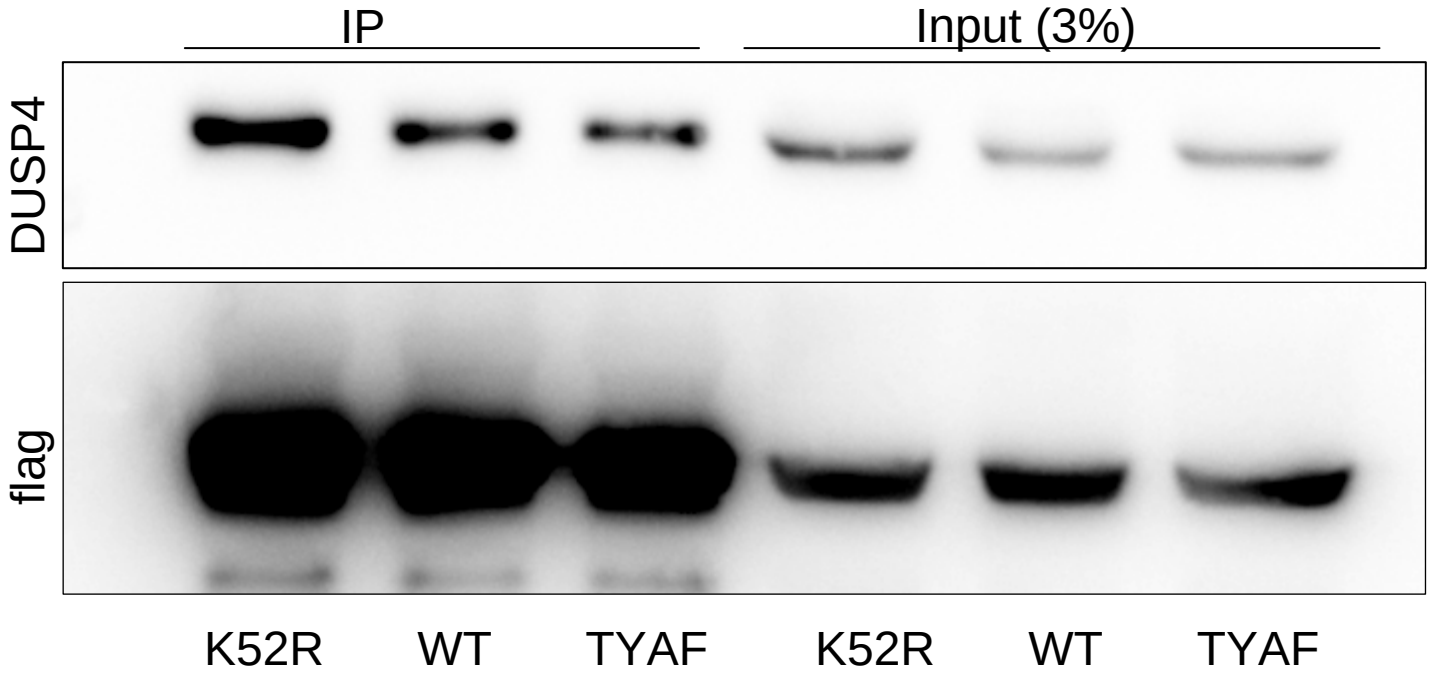

Figure S11-R